Journal of Hydrology: Regional Studies 46 (2023) 101338

Contents lists available at ScienceDirect

Journal of Hydrology: Regional Studies

journal homepage: www.elsevier.com/locate/ejrh

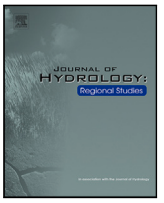

Shifted discharge and drier soils: Hydrological projections for a Central Asian catchment

Timo Schaffhauser [a,*], Stefan Lange [b], Ye Tuo [a], Markus Disse [a]

[a] Technical University of Munich School of Engineering and Design, Technical University of Munich, Munich, Germany
[b] Potsdam Institute for Climate Impact Research, Potsdam, Germany

ARTICLE INFO

Keywords:
Hydrological modeling
SWAT
Climate impact assessment
Soil moisture evapotranspiration coupling
Central Asia
ISIMIP

ABSTRACT

Study Region

The Naryn River Basin, Kyrgyzstan

Study Focus

We investigate the impacts of climate change in the basin based on two families of General Circulation Models (GCMs) using the hydrological model SWAT. The forcing datasets are the widely used ISIMIP2 (I2) and the newly derived ISIMIP3 (I3) data which refer to the 5th and 6th stage of the Coupled Model Intercomparison Project (CMIP). Due to notable differences in the forcing we evaluate their impacts on various hydrological components of the basin, such as discharge, evapotranspiration (ETA) and soil moisture (SM). Besides, a partial correlation (PC) analysis is used to assess the meteorological controls of the basin with special emphasize on the SM-ETA coupling.

New Hydrological Insights for the Region

Agreement in the basin's projections is found, such as discharge shifts towards an earlier peak flow of one month, significant SM reductions and ETA increases. I3 temperature projections exceed their previous estimates and show an increase in precipitation, which differs from I2. However, the mitigating effects do not lead to an improvement in the region's susceptibility to soil moisture deficits. The PC study reveals enhanced water-limited conditions expressed as positive SM-ETA feedback under I2 and I3, albeit slightly weaker under I3.

1. Introduction

Central Asia (CA) is characterized by unevenly distributed renewable water resources and is prone to water-related conflicts (Bernauer and Siegfried, 2012; Berndtsson and Tussupova, 2020; Peña-Ramos et al., 2021). Water availability originates mostly from the high-mountainous part and relies to a significant part on nivo-glacial processes that supply water to the arid lowlands where it is used for agricultural production or to satisfy the energy demand (Didovets et al., 2021; Chen et al., 2016; Hagg et al., 2007). Central Asian's water towers are vulnerable to climate change, due to glacier recession and seasonal snow cover reductions which will lead to substantial impacts on the freshwater availability of the local population (Barandun et al., 2020, 2021; Huss and Hock, 2018; Saks et al., 2022). Further, climatic changes are already expected to exacerbate droughts, with partly adverse effects and risks on vegetation and ecosystems (Jiang et al., 2017; Zhou et al., 2015; Xing et al., 2022). CA is particularly vulnerable to land degradation, especially with its special form of desertification, which is already present and might be more pronounced in the future due to further climatic changes (Huang et al., 2020a; Zhang et al., 2018; Li et al., 2015). Reasons can be a multitude of climatic

* Corresponding author.
E-mail address: t.schaffhauser@tum.de (T. Schaffhauser).

https://doi.org/10.1016/j.ejrh.2023.101338
Received 31 August 2022; Received in revised form 18 January 2023; Accepted 4 February 2023
Available online 23 February 2023

effects, such as precipitation decrease reducing moisture availability or temperature increases enhancing evapotranspiration as well as anthropogenic causes (Jiang et al., 2022; Peng et al., 2021). However, the relationships between these factors and the vegetation response are complex and challenging (jie Xu et al., 2016; Gessner et al., 2013).

Non-climatic factors such as mismanagement of water resources as it was the case for the prominent example of the Aral Sea Basin (Xenarios et al., 2018; Hamidov et al., 2016) and the general drivers of water stress in transboundary river basins, such as allocation, upstream water use or damming exacerbate water-related issues (Hill et al., 2017; Wilson et al., 2017; Döll et al., 2009).

Reported observed temperature rises range from 0.2–0.3 °C per decade (1956–2007) in the Tian Shan (Kutuzov and Shahgedanova, 2009) up to 0.36 ° 0.42 °C (1979–2011) per decade considering whole Central Asia (Hu et al., 2014). There is also evidence that the warming trends were intensified since the 1970s, while for precipitation observed changes are more heterogeneous without consistent patterns (Unger-Shayesteh et al., 2013). Climate projections in the context of the fifth phase of the Coupled Model Intercomparison Project (CMIP5) project significant temperature increases until 2099, e.g. Immerzeel et al. (2013) reports a temperature rise of around 2 °C until 2050 under the RCP4.5 (Relative Concentration Pathway) for the Amu Darya and Syr Darya, which is consistent with the calculated increase of 1–2.2 °C in High Asia by Lutz et al. (2014). Ozturk et al. (2017) estimates a temperature increase of up to 7 °C under the high emission scenario RCP8.5 until 2099, which is in line with the projected changes in Summer of 6.5 °C in Reyer et al. (2015). Precipitation trends are mostly minor and show a strong spatial diversity. Besides, precipitation changes are less significant and more uncertain for most projections (Lutz et al., 2014; Immerzeel et al., 2013; Luo et al., 2018). Only Ozturk et al. (2017) reports a more consistent precipitation decrease in their study.

More recent studies which are based on the newer Shared-Socioeconomic Pathways (SSP) and newer General Circulation Models (GCM) from CMIP6 show strong similarities in projected temperatures with slightly higher projections compared to CMIP5. Under SSP8.5 Lalande et al. (2021) calculated an upper bound of 9 °C for the adjacent located High Mountain Asia (HMA). A different picture is found for precipitation changes over CA, where several studies report a clear increase in precipitation amounts, with ranges from 10.5%–14.4% under SSP2.6 and SSP8.5 until the end of the century (Jiang et al., 2020) or similar findings (Guo et al., 2021). However, CMIP6-based impact studies that investigate what these differences in the new estimates could mean are still rare but will likely increase in the near future.

The assessment of climate change impacts on different components, e.g. of the hydrological cycle is an essential element for the development of societal adaption and mitigation strategies but also to raise the general awareness of potential changes. However, climate impact studies are subject to a complex modeling chain, considering multiple scenarios, multiple GCMs (multi-model), downscaling and bias-adjustment methods and lastly an impact model such as an hydrological model (Huang et al., 2020b; Olsson et al., 2016). As a consequence impact studies are prone to large uncertainties initiated by these different sources (Wen et al., 2020; Bosshard et al., 2013). Nevertheless, the quantification and communication of uncertainties play an important role in impact modeling (Mishra et al., 2020; Vetter et al., 2015), where one aim should be the minimization of uncertainty referred to the impact model to improve the reliability of the projected changes (Vetter et al., 2016; Krysanova et al., 2018). Thus, Krysanova et al. (2020) showed in their special issue how a robust impact model can reduce the magnitude of projected uncertainties and provided guidelines for a comprehensive model evaluation in addition to the standard calibration and validation procedure.

Due to the importance of CA's water towers and its dependence on agriculture the evaluation of its climate and hydrology is essential for adaption and mitigation. Climate impact assessment on the hydrological cycle in CA has been conducted in several studies, as it was done for eight CA catchments by Didovets et al. (2021) with varying results depending on the catchment characteristics and flow regime. Gan et al. (2015) reports a shift towards earlier peak discharge and runoff as well as precipitation declines in the Naryn Catchment. Slight reductions in runoff combined with similar significant seasonal shifts are found by Hagg et al. (2013) for the Upper Amu Darya. More substantial negative changes in runoff are estimated for the Chu River Basin by Changkun et al. (2015).

However, climate impact studies on the hydrological cycle based on CMIP6 are almost not available in the region. Thus, our aim is to provide an assessment of climate change impacts on different hydrological components within the Naryn Basin considering a subset of the recent CMIP6 GCMs and scenarios. Secondly, we do not solely focus on the climate projections based on CMIP6 but reveal how the impacts on the hydrological cycle changed from CMIP5 to CMIP6, which is particularly relevant in the context of adaptation and mitigation strategies. Our GCM subsets are derived from the Inter-Sectoral Impact Model Intercomparison Project (ISIMIP) versions 2b and 3b and will be designated as I2 and I3 in the following (see 2.1). Special emphasize is put on the differences in the projected coupling of soil moisture and evapotranspiration, initiated through disparate precipitation and temperature projections between the two generations. Hence, we perform a correlation analysis, where a partial correlation (PC) system is used to assess the meteorological effects on and changes within the soil moisture-evapotranspiration feedback.

2. Materials and Methods

2.1. Datasets used in this Study

We used the daily meteorological data of four GCMs and two scenarios from CMIP5 for the analysis of future changes and the corresponding successor models and scenarios from CMIP6 to drive our hydrological model and to evaluate how projected impacts differ between both CMIP generations. In total then 8 GCMs were utilized, 4 of each generation of climate models. In detail we used the GCM data from GFDL-ESM2M, HadGEM2-ES, IPSL-CM5A-LR and MIROC5 under CMIP5 and the corresponding successor GCMs GFDL-ESM4, UKESM1-0-LL (successor of HadGEM2-ES), IPSL-CM6A-LR and MIROC6 under CMIP6, respectively. The selected

Table 1
Overview of used datasets.

Variable/Data type	Abbreviations	Datasets	References
Temperature, precipitation	T, P	EWEMBI, W5E5	Lange (2018), Cucchi et al. (2020), Lange et al. (2021)
Evapotranspiration	ETA	GLEAM V3.5	Miralles et al. (2011), Martens et al. (2017)
Soil moisture	SM	GLDAS Noah V2.1	Rodell et al. (2004)
Digital elevation model	DEM	SRTM90	NASA JPL (2013)
Land use	–	ESA CCI-LC	ESA (2017)
Soil	–	HWSM	FAO, IIASA, ISRIC, ISSCAS, JRC (2012)
Climate projections/models	I2, I3	ISIMIP2b:GFDL-ESM2M, HadGEM2-ES, IPSL-CM5A-LR, MIROC5 ISIMIP3b: GFDL-ESM4, UKESM1-0-LL, IPSL-CM6A-LR, MIROC6	Frieler et al. (2017), Lange (2018, 2019)

Note: The climate projections of ISIMIP2b and ISIMIP3b belong to CMIP5 and CMIP6, respectively.

scenarios refer to a low and high emission scenario of both phases, namely RCP2.6, RCP8.5 and SSP1-2.6 as well as SSP5-8.5, respectively. In the following we denote them simply as RCP26, RCP85, SSP26, SSP85.

The data was obtained from the ISIMIP project, where the GCM data was separately downscaled and bias-adjusted for each CMIP phase. ISIMIP is (analogously to CMIP) structured in various phases, where ISIMIP2b (Frieler et al., 2017; Lange, 2018) corresponds to CMIP5, while ISIMIP3b (Lange, 2019) utilizes CMIP6 results. The ISIMIP2b procedure preserves trends in long-term mean values using adjustment factors or offsets for those statistics and transfer functions for the adjustment of day-to-day variability around the monthly mean value. In contrast, the ISIMIP3b procedure adjusts biases using quantile mapping and preserves trends in all quantiles of the distribution of a climate variable. Statistical downscaling is done via spatial interpolation in ISIMIP2b and with multivariate quantile mapping in ISIMIP3b. Furthermore, the bias-adjustment was performed for different reference datasets, namely EWEMBI under ISIMIP2b (CMIP5 GCMs) (Lange, 2018) and W5E5 under ISIMIP3b (CMIP6 GCMs) (Cucchi et al., 2020; Lange et al., 2021) providing the base for the calibration and validation of our hydrological model. Both reference datasets were designed for the bias-adjustment of climate impact studies. Both datasets merge various data sources, EWEMBI hereby is based on EartH2Observe forcing, ERA-Interim, NASA/GEWEX Surface Radiation Budget data and WFDEI data. The predecessor W5E5 combines the methodology of version 1.0 WATCH Forcing Data, ERA5 reanalysis data, and precipitation data from version 2.3 of the Global Precipitation Climatology Project. The two reference datasets are the base for the bias-adjustment of the corresponding ISIMIP phase (see Table 1).

To evaluate simulated actual evapotranspiration (ETA) and soil moisture (SM) of SWAT, we considered the widely used data from the Global Land Evaporation Amsterdam Model (GLEAM) (Miralles et al., 2011; Martens et al., 2017) and Global Land Data Assimilation System (GLDAS) (Rodell et al., 2004), respectively.

The Digital Elevation Model (DEM) with a resolution of 90 m was acquired from the Shuttle Radar Topography Mission (SRTM) (NASA JPL, 2013). Land use data was obtained from the European Space Agency's Climate Change Initiative Land Cover (ESA CCI-LC) project (ESA, 2017) with a resolution of 300 m and soil data was received from the Food and Agricultural Organization's (FAO) 1 km Harmonized World Soil Map (HWSM) (FAO, IIASA, ISRIC, ISSCAS, JRC, 2012). As the used ISIMIP data represents only a subset of available GCMs of each CMIP generation it has to be noted that our approach rather compares a sample of each CMIP generation based on the ISIMIP data than providing a complete picture, which was beyond the scope of that study.

2.2. Study area - Naryn Basin

The Naryn Basin is located in Kyrgyzstan and is, along with the Kara Darya one of the two headwater catchments of the Syr Darya River in the Aral Sea Basin. The Naryn is formed by the two headwater rivers, Big and Small Naryn, which originate in the Tian Shan mountains. It flows westwards through Kyrgyzstan until it crosses the border to Uzbekistan, where it joins the Kara Darya in the Fergana Valley. The basin is characterized by a nivo-glacial flow regime, where the flood period begins in April and ends in September. The catchment size is around 58,000 km^2, however our study only considers the share of the catchment (~46,000 km^2) until the Toktogul Reservoir, a multi-purpose reservoir used for hydroelectricity generation and irrigation. Around 2.2% of the catchment is glacierized, where the majority of the glaciers lie in the Eastern area.

The region has a dry continental and semi-arid climate with annual precipitation sums between 280 mm–450 mm (Aizen et al., 1995). Depending on the location and elevation within the basin, the annual maximum precipitation occurs in Spring or Summer. Temperatures are diverse throughout the basin and the mean Summer temperatures can reach 25 °C and during the Winter months the mean temperatures can fall down to −20 °C. An overview of the study area can be found in Fig. 1.

2.3. Hydrological model — SWAT

The Soil Water Assessment Tool (SWAT) is a process-based, semi-distributed and continuous model which was developed by the Blackland Research & Extension Center of the United States Department for Agriculture (USDA) (Arnold et al., 1998). SWAT was initially developed to evaluate the impact of land management practices in large watersheds, but is nowadays used for a multitude of applications all over the world. SWAT is widely used for sediment studies, water resources management, climate impact assessment or agricultural investigations (Arnold and Fohrer, 2005).

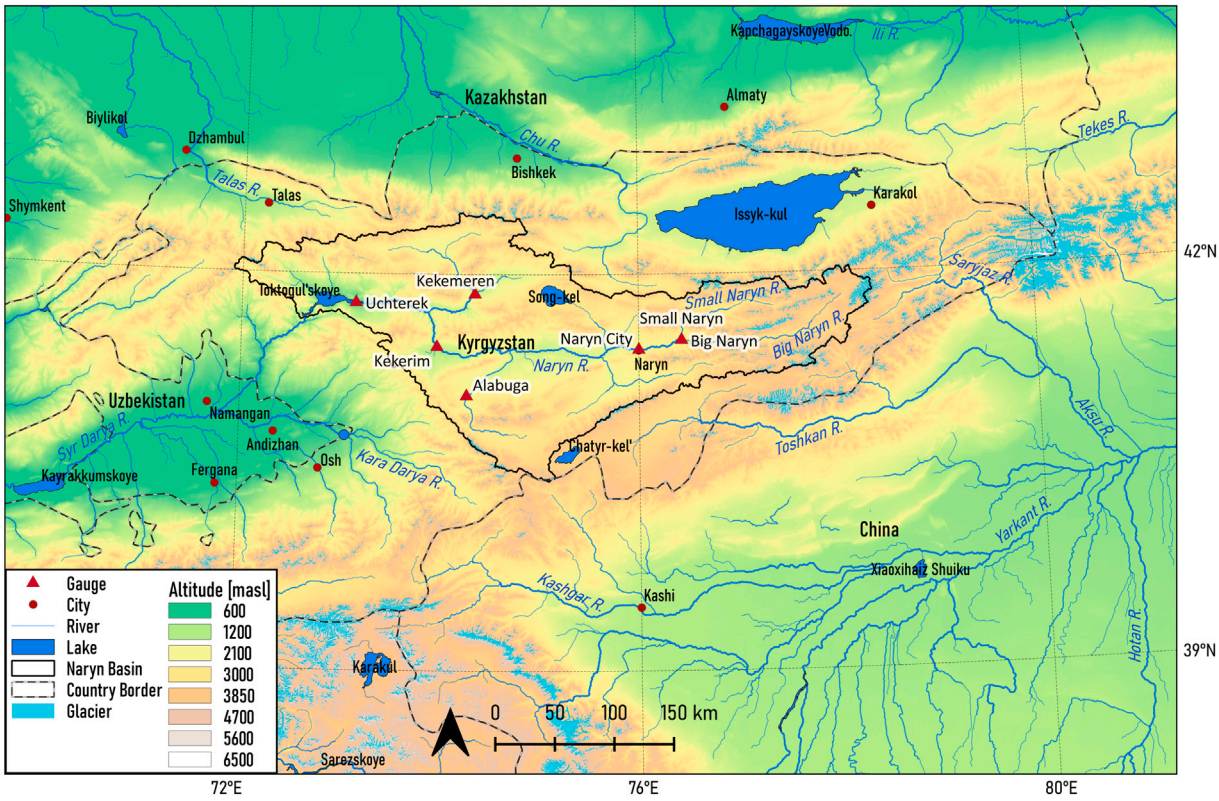

Fig. 1. Overview of the Naryn Basin within Kyrgyzstan. The gauges refer to the subcatchments which were used for the multi-site calibration of this study. The gauges of the Small and Big Naryn are only a few meters apart (just before their confluence) and thus share one symbol.

Spatially, the catchment is subdivided into subbasins, on the basis of which a further spatial discretization into Hydrological Response Units (HRUs) takes place. The latter one serves as the smallest spatial unit within the model and represents a unique combination of land use, soil and slope on the subbasin level. Computations are divided into a land and a water phases, where the calculations of the land phase are carried out on the HRU level. The land phase hereby covers the processes which are responsible for the movement of water, nutrients or sediment to the stream of a subbasin. SWAT first sums up the area dependent HRU loadings and fluxes of each subbasin before they are transferred to the corresponding stream. The water or routing phase refers to instream processes, such as the transport of water, sediment or nutrients through the channel network.

2.4. Calibration, validation and evaluation test

This section describes the calibration and evaluation procedure of the hydrological model based on the reference datasets of both projection families. The approach follows the suggestions of Krysanova et al. (2018, 2020) and some modifications provided in Gelfan et al. (2020). The whole methodology is represented in Fig. 2. For each of the two reference datasets of the ISIMIP phases a SWAT model was set up individually. In detail we performed the following steps, (1) multi-site calibration of seven gauges considering multiple goodness of fit criteria (GOF) (Fig. 2a), (2) model robustness check under contrasting climate periods (Fig. 2b), (3) cross-evaluation of model robustness using evapotranspiration and soil moisture estimates (Fig. 2b). First, the procedure was applied for the SWAT model forced with the EWEMBI reference dataset (representing I2), before we transferred the obtained parameter set to the W5E5 (representing I3) driven impact model and the same steps were performed again. Only if all steps for both hydrological models (forced with the two reference datasets of I2 and I3) could be carried out satisfactorily, the impact assessment is conducted. Due to inconsistencies in data availability and quality, daily discharge data was only available for four gauges and monthly data was obtained for the three remaining gauges. Based on the available data the calibration period was set to 1974–1981 and the validation period from 1982–1987 for the EWEMBI driven model. A limitation arose through different temporal coverages of EWEMBI and W5E5. Originally, both datasets are available from 1979 onward. However, for EWEMBI the extended GSWP3-EWEMBI (hereafter EWEMBI) product enabled a prolonged temporal coverage. A similar extension was not accessible for the W5E5 dataset at the time the calibration was done. Therefore the calibration period was set to the validation period of the model driven with EWEMBI. Due to these limitations a separate and suitable validation phase could not be used. As a preliminary study the two forcing datasets were compared and evaluated to quantify differences in the basin.

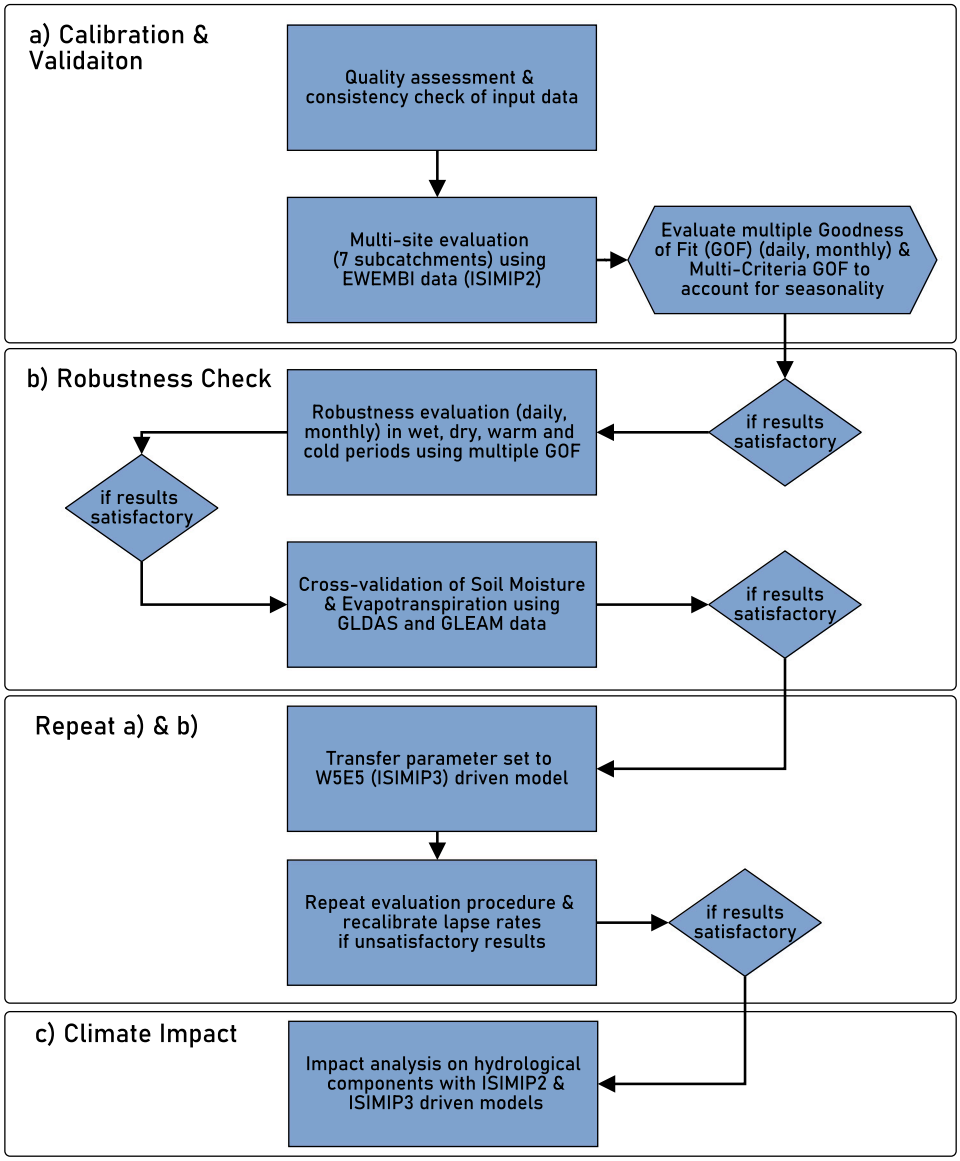

Fig. 2. Flowchart showing the methodology of our study based on the comprehensive evaluation test proposed by Krysanova et al. (2020). The study is structured in three blocks, the calibration and validation, the robustness check followed by the final impact assessment. The multiple Goodness of Fit (GOF) correspond to Nash–Sutcliffe Efficiency (NSE), Kling-Gupta Efficiency (KGE), Root Mean Square Error (RMSE) and Percent Bias (PBIAS).

Step 1 of the procedure considered multiple rules: We calibrated from upstream to downstream and for each gauge multiple initial simulations were performed to close the water balance. The number varied throughout the subcatchments based on how fast the water balance could be closed. Multiple GOF criteria were selected during the calibration procedure. The water balance closure was assessed based on the Percent Bias (PBIAS), where we adapted and fixed the lapse rates for temperature and precipitation. Secondly, different parameter groups were calibrated (e.g. snow parameters, groundwater parameters etc.) and evaluated using the Nash Sutcliff Efficiency (NSE), Kling Gupta Efficiency (KGE) in combination with a seasonal RMSE to account for a trade off between daily/monthly and seasonal results. An overview of the selected parameters and their categories is presented in A.1.

When satisfactory results in the calibration and validation phase were achieved, a robustness check for contrasting climatic conditions was performed (step 2).

The model performance is evaluated against wet and dry years, as well as for warm and cold years, by forming a sequential time series of non-continuous years. Each sequence then represents the respective climate. Thus, the mean annual precipitation and temperature for the calibration and validation period were calculated. Each year was then individually divided by the mean value and either classified as cold if the mean temperature of a year, Ti (where i is the individual year) is smaller than the mean annual

temperature of the whole time series, $Tmean$, (or warm if $Ti > Tmean$), and wet if the annual precipitation of a year, Pi, > the mean annual precipitation of the time series, $Pmean$ (or dry if $Pi < Pmean$). The four resulting discharge time series per SWAT model were then evaluated with the GOF criteria introduced under step 1.

Lastly (step 3), a cross-evaluation using ETA data from GLEAM as well as SM from GLDAS is performed to ensure an adequate internal model consistency and to represent various components of the hydrological system (Krysanova et al., 2020). The analysis was done on the basin and subbasin scale for monthly and annual estimates. The performance of ETA is illustrated by means of the NSE, RMSE and the Pearson Correlation r. However, SM could not been validated in absolute values due to a mismatch in the soil layer definitions within the SWAT model and GLDAS, which provides SM values for different layers (e.g. 0–10 cm or 10–40 cm). Thus, we rather assessed seasonal and inter-annual SM anomalies, again by a (r) coefficient and a normalized version of the RMSE (NRMSE), computed by a normalization with the interquartile range (difference between 75th percentile and 25th percentile). Similar difficulties with SM evaluations are presented for example in Poméon et al. (2018), Rajib et al. (2016) and Dembélé et al. (2020).

To allow for an appropriate comparison of the impacts based on the I2 and I3 driven models, we aimed for a consistent parameterization of both models. Thus, steps 1–3 were first performed for the SWAT model driven with EWEMBI and then, when satisfactory results were achieved, the same parameterization was used for the model forced with W5E5. Then all three steps were carried out again. A final parameterization was stated as acceptable when similar results are obtained for both models. However, due to minor differences in the forcing datasets (EWEMBI and W5E5) in their mean annual precipitation and temperature, minor adaptions in the parameterization were necessary to match the water balance. The adaptions were thus limited to the lapse rates and in seldom cases to the snow pack temperature lag factor.

2.5. Projected changes of ISIMIP2b and ISIMIP3b

This section illustrates the comparison between both generations of projections. First, we show how the temperature and precipitation projections as well as their estimates in the historical phase differ. The comparison is done on the basin scale for multiple temporal representations (seasonal, annual). The future projections are derived from the four general circulation models of each projection phase (I2 and I3, respectively) and scenario. In order to ensure an adequate comparability, we selected GCMs that are both available in I2 as well as in the new phase I3, represented by a corresponding successor model (see 2.1). Accordingly, we focused on CMIP5's RCP scenarios that were translated and continued by a corresponding SSP scenario that characterizes a similar aggregated forcing. However, there are several differences between the RCP scenarios and their successors, which are explained and demonstrated in detail in Meinshausen et al. (2020) or Tebaldi et al. (2021). This assumption leads to the consideration of the low emission (RCP2.6 and SSP2.6) and high emission (RCP8.5 and SSP8.5) scenarios. As SWAT requires $Tmax$ as input, we use the respective quantity as proxy for mean daily temperature changes. Precipitation changes ΔP refer to relative anomalies of the mean annual sum.

2.5.1. Differences in meteorological forcing

First of all we present the differences in the meteorological variables of all GCMs between I2 and I3. Therefore we calculate anomalies of two future 30-year periods, near (2020–2049) and far future (2070–2099), to the historical baseline period (1971–2000). Differences are illustrated individually for precipitation and temperature as multi-model mean (MMM) of the GCMs of each ISIMIP phase. Uncertainties are represented as GCM range. The radiative forcings of the selected scenarios of I2 and I3 are equal (e.g. SSP85 similar to RCP85). Deviations arise mainly from different climate sensitivities present in the GCMs of the different CMIP or ISIMIP phases.

2.5.2. Changes in hydrological components

As a next step, future hydrological changes in the basin are evaluated as a result of the various trajectories. Therefore, discharge, ETA and SM anomalies are assessed for the I2 and I3 forced hydrological models and compared afterwards. The model spread provides a representation of the uncertainty, and the ensemble mean represents the average future change per scenario and generation of projection. Analogously to the meteorological changes, hydrological changes are presented on a basin scale as seasonal and annual anomalies.

2.6. Meteorological controls of the soil moisture and evapotranspiration feedback

Special emphasize is put on the relevance of meteorological drivers on variations in SM and ETA as well as the future development of the ETA-SM feedback under both generation of climate models. It was aimed to evaluate to what extent meteorological differences under I2 and I3 affect the coupling of SM and ETA. The interaction is implicitly considered in the model (non-linear decrease when SM is below field capacity). To identify the major controls and their effects on the SM-ETA feedback, a partial correlation system was developed, which gives further insights on the direction and strength of the SM-ETA mechanism. The evaluation focused on the MMM results of the GCMs (e.g. the MMM for each variable of a specific scenario and time period within the corresponding ISIMIP phase) to draw conclusions with regard to the mean signal. For the analysis monthly anomalies of the meteorological and hydrological variables were generated.

Since ETA and SM variations are larger during the vegetative season (which partly coincides with the rainy season, see Fig. A2), the analysis was based on the period from April to September. The vegetation season is thus assumed to be stationary until 2099

and potential phenological shifts are not considered. For the analysis the vegetative season was split in two periods, April–June (AMJ) which roughly coincides with the rainy season in the basin and July to September (JAS), which is generally drier on the basin scale. It has to be noted that irrigation, which is the largest water consumer of Kyrgyzstan, was not explicitly considered in the simulations. The PCs allow to directly control for the effects of one or more independent variables to identify confounding effects (variable that explain part of the relationship which is present in the standard regression between a dependent and independent variable). We thus considered the combined effects of temperature, precipitation, SM and ETA to infer potential future shifts in the SM-ETA interaction and their dominant controls. In our case combined effects refer to the consideration of two control variables, e.g. in the PC calculation between temperature and SM, the effects of the remaining variables ETA and precipitation are taken into account. Accordingly, the PC calculation is supported by the standard Pearson correlation values to highlight the confounding effect. A significant shift in the correlation values (Pearson and PC value) indicates that the relationship cannot be explained by one driver alone, but is partly based on the second variable. ETA variations are assessed by the explanatory strength of temperature and SM, while SM was evaluated using temperature. Since SM generally controls ETA in water-limited regimes and not vice versa, we present the SM-ETA coupling in the PC system of ETA rather than SM (Berg and Sheffield, 2019). Mathematically, the PC system can be formulated as follows:

$$r_{yx_1,x_2} = \frac{r_{yx_1} - r_{yx_2} r_{x_1x_2}}{\sqrt{(1 - r^2_{yx_2})(1 - r^2_{x_1x_2})}} \tag{1}$$

where, r_{yx_1,x_2} refers to the partial correlation coefficient between the dependent variable y (SM or ETA) and the independent variable x_1, while controlling for the effects of the independent variable x_2, the remaining r represent the Pearson correlation coefficients between the corresponding pairs of variables. The control variables can be precipitation, temperature, SM or ETA. E.g., if we want to evaluate potential effects of precipitation, the control variable x_2 would refer to precipitation and x_1 to temperature. Hence, $r_{x_1x_2}$ would refer to the Pearson correlation of precipitation and temperature.

3. Results

Hereafter, we present the results of the calibration procedure, the comparison of projected meteorological and hydrological changes under the new and old climate model generations, the relevance of the meteorological controls and the findings of the uncertainty decomposition.

3.1. Calibration, validation and evaluation test

The following sections correspond to part a) and b) illustrated in Fig. 2. Statistical results (w.r.t. different GOF criteria) for all seven gauges are presented in Table 2. Note, due to unsatisfactory data availability there is no validation phase for W5E5 (see 2.1).

Apart from the Big Naryn Basin, a significant deterioration between the monthly and daily calibration results, as well as between EWEMBI and W5E5 could not be detected. Best results were achieved at the basin outlet. On average the NSE values are around 0.75 for the calibration and validation period (KGE 0.82, PBIAS 9.4%) in the two models. Worst results are found at the two headwater streams Big and Small Naryn. The poorer results here are likely to be caused by the higher relevance of glacier processes, which were not represented by the model. A comprehensive discussion on that can be found in the discussion section at the end of this work. Besides, a notable difference in water volumes (expressed as PBIAS) was found at gauge Kekirim, which is caused by a systematic overestimation of late Summer and Autumn flow (July–October). Fig. 3 shows the daily/monthly calibration and validation results for four selected gauges combined with their seasonal hydrographs. We selected one gauges which was calibrated monthly and three daily calibrated gauges to emphasize the comparable performance. For the daily calibrated gauges the selection comprised two well-performing gauges followed by the Big Naryn where poorer results were achieved. In general, both daily/monthly and seasonal hydrographs of both models show a good agreement with the observed flow with the exception of the Big Naryn. In general, the model based on EWEMBI data as well the one driven with W5E5 are able to reproduce the seasonal behavior within the respective subcatchments. However, in case of the poorer performing headwater catchment it becomes apparent that the deterioration is likely caused by a mismatch during summer where a systematic underestimation occurs. The mean seasonal plots include observed flow for two different periods, each representing the maximum available data of EWEMBI (1974–1987) and W5E5 (1982–1987), respectively.

The robustness check, in which the model performance was individually assessed in wet/dry and warm/cold periods (see Section 2.4), led to comparable results as achieved in the original calibration and validation procedure. The results of the evaluation for all gauges can be found in Table 3. Overall, wet periods are better reproduced by both models for both GOF criteria than dry years (NSE_{wet} 0.8, NSE_{dry} 0.7, $PBIAS_{wet}$ ±9%, $PBIAS_{dry}$ ±11.8%). Also for warm and cold phases, model performances are similar (NSE_{warm} 0.75, NSE_{cold} 0.71 and $PBIAS_{warm}$ ±9.1%, $PBIAS_{cold}$ ±10.46%). The numbers are average values of both models and all gauges. Similar to the original calibration, the same gauges exhibit the worst performance.

Comparing the robustness of the EWEMBI and W5E5-driven models, no significant differences are observed. The model forced by EWEMBI data performs better in warm periods, slightly better in dry periods, similar in wet periods and slightly worse in cold years compared to its W5E5 counterpart. It can be concluded that the methodology is generally able to produce comparable results for both models. In overall, the models performed reasonable for most of the gauges in all climate phases, as well as for the standard calibration and validation procedure and thus successfully pass the first two steps of the evaluation test.

Gauges that produced unsatisfactory results are in line for both models, indicating the similarity in the parameterization and the meteorological forcing of both reference datasets. Poor results relate mainly to the Big Naryn and gauge Kekerim, where the poor performance mainly arises from water balance issues (indicated by PBIAS). A notable deterioration of the results is found in the Small Naryn Basin when moving from EWEMBI to W5E5. In contrast, an improvement is even obtained at gauge Kekerim.

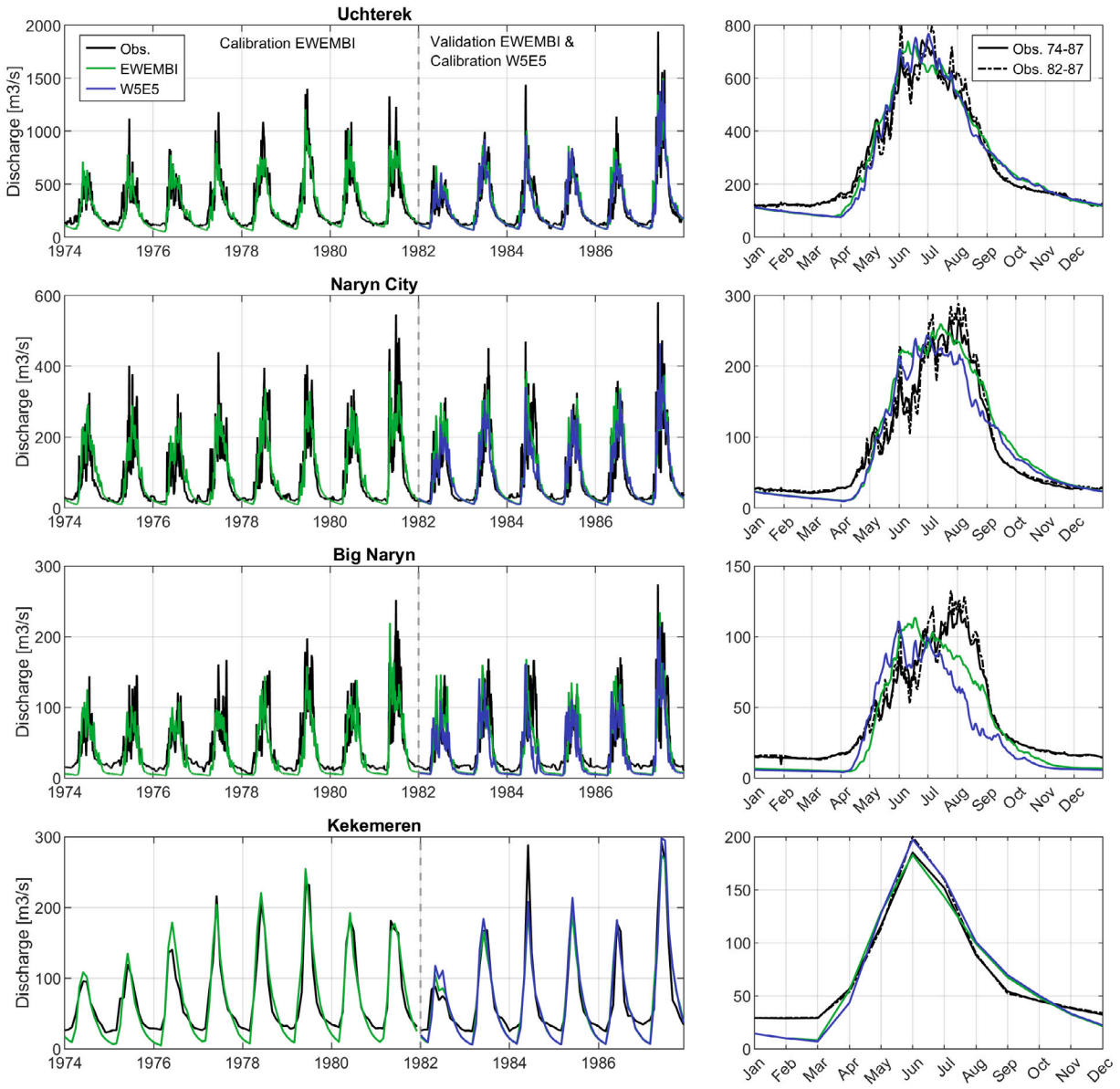

Fig. 3. Calibration and validation results for four selected gauges. Gauge Uchterek, Naryn City and Big Naryn were calibrated on a daily scale. Kekemeren is based on a monthly calibration due to limited data availability. Note, for the period 1974–1981 only the extended EWEMBI dataset was available. Plots in the right column show the mean seasonal flow for the period 1974–1987 (calibration & validation phase of EWEMBI) and 1982–1987 (calibration phase W5E5): black lines — observed flow of the indicated periods, blue lines — W5E5 simulated flow 1982–1987, green lines — EWEMBI simulated flow 1974–1987. (For interpretation of the references to color in this figure legend, the reader is referred to the web version of this article.)

3.1.1. Cross-validation of actual evapotranspiration

To improve the models reliability, they were cross-validated with respect to the GLEAM ETA product in order to increase the credibility of the projected changes. The cross-validation is performed to assure consistency of the hydrological processes within the catchment and to further improve model robustness. Due to the data availability it was performed from 1982 to 1987.

The simulated ETA of both models show a high agreement with the ETA estimates of GLEAM. At the catchment scale, a NSE of 0.97 is achieved based on the monthly evaporation estimates for the EWEMBI-forced model (RMSE = 4.1 mm, PBIAS = 3.2%). The performance of the W5E5-driven model is similar with a NSE of 0.96 (RMSE = 4.6 mm, PBIAS = 3.3%). Basin values for r are almost 1. On the subbasin scale the median NSE and r value are > 0.8 and > 0.9, respectively, for both models without any significant difference between them. NRMSE values are close to 0 for both models with both medians around 0.20. However, the small number of subbasins performing poor arises from both, a systematic over- and underestimation of SWAT in the Summer period, without any

Table 2
Calibration and validation results for the final parameter set used for the climate impact study. The last three gauges refer to the gauges where no daily discharge data was available and the calibration was performed on a monthly scale. Note that the calibration period for EWEMBI was 1974–1981 (validation period (1981–1987, while it was 1981–1987 for W5E5 (no validation phase) due to insufficient data.

Gauge	NSE [-]			KGE [-]			PBIAS [%]		
	Calibration		Validation	Calibration		Validation	Calibration		Validation
	EWEMBI	W5E5	EWEMBI	EWEMBI	W5E5	EWEMBI	EWEMBI	W5E5	EWEMBI
Uchterek (46,440 km^2)	0.83	0.87	0.84	0.9	0.93	0.92	3.67	2.97	−2.35
Naryn City (10,291 km^2)	0.74	0.74	0.72	0.84	0.84	0.82	−5.53	3.67	−10.79
Big Naryn (5529 km^2)	0.59	0.45	0.58	0.73	0.63	0.77	18.97	26.76	11.31
Small Naryn (3877 km^2)	0.78	0.59	0.63	0.84	0.62	0.81	5.38	21.29	−7.55
Alabuga (3718 km^2)	0.83	0.78	0.75	0.91	0.84	0.79	−3.82	5.6	−4.79
Kekerim (1715 km^2)	0.65	0.89	0.79	0.71	0.88	0.79	−26.27	−9.57	−12.92
Kekemeren (8199 km^2)	0.89	0.88	0.88	0.85	0.91	0.91	2.81	4.33	6.91

Table 3
Results of the robustness check for wet/dry and warm/cold years under consideration of the whole simulation period (calibration with validation phase) for the model driven with EWEMBI. For the W5E5-based model the periods were formed within the period 1982–1987, due to limited data.

Gauge	NSE [-]								PBIAS [%]							
	EWEMBI				W5E5				EWEMBI				W5E5			
	Wet	Dry	Warm	Cold	Wet	Dry	Warm	Cold	Wet	Dry	Warm	Cold	Wet	Dry	Warm	Cold
Uchterek	0.86	0.8	0.88	0.82	0.88	0.84	0.84	0.88	−5.5	−5.18	3.95	−2.11	−4.37	7.39	2.7	3.1
Naryn City	0.78	0.69	0.78	0.66	0.8	0.7	0.8	0.71	−5.7	−9.22	−2.28	−14.01	−4.18	7.95	−0.96	5.89
Big Naryn	0.66	0.5	0.62	0.55	0.62	0.3	0.53	0.42	15.75	15.55	19.69	11.27	23.04	28.95	26.49	26.90
Small Naryn	0.7	0.73	0.81	0.56	0.65	0.56	0.65	0.55	−6.8	3.48	8.17	−10.01	−6.11	32.29	21.37	21.25
Alabuga	0.86	0.71	0.87	0.68	0.85	0.74	0.69	0.77	−7.97	−1.64	−1.31	−7.5	−7.72	−0.59	13.67	5.55
Kekirim	0.77	0.67	0.75	0.72	0.82	0.71	0.89	0.9	−20.6	−19.65	−18.89	−21.34	−17.46	−19.5	3.03	−9.01
Kekemeren	0.9	0.87	0.91	0.87	0.9	0.88	0.53	0.89	0.82	7.23	4.32	4.93	0.18	6.63	−0.24	3.56

clear pattern. Due to the high agreement between the ETA estimates of both models and an overall very good performance, results are considered satisfactory.

Fig. 4 summarizes the monthly results on the basin and subbasin scale, where the latter is represented as boxplot for the individual performance metrics.

3.1.2. Cross-validation of soil moisture

Similar to ETA, the SM estimates of the two SWAT models were evaluated using GLDAS data. The performance was assessed for soil moisture anomalies. We also used a NRMSE due to different soil layer assumptions (see Section 2.4). Analogously, the evaluation period was from 1982 to 1987.

It was found that the resulting SM estimates of both models (based on the reference datasets EWEMBI and W5E5) reveal a satisfactory agreement on the basin scale. Besides, the general seasonal behavior in the models is reproduced in a satisfactory way with respect to the GLDAS SM, particularly at the basin scale. On the basin scale the NRMSE is 0.44 for the EWEMBI and W5E5-driven model, respectively. In addition, a r-value of 0.81 is obtained for both models. The basin NSE is 0.65 for the model forced with EWEMBI and 0.64 for the one based on W5E5.

On the subbasin scale the median (considering the performance of all individual subbasins) NRMSE is 2.20 (r = 0.62) for the EWEMBI-driven model and 2.24 (r = 0.62) for the W5E5 counterpart (see Fig. 4). However, on the subbasin scale a deterioration in all evaluation metrics can be observed, which is mainly due to the very poor performance of some subbasins. While the deficiencies are counterbalanced on the basin scale, some subbasins proved to produce much stronger seasonal cycle, which were not found in the GLDAS estimates. The effect is reflected in the weaker NSE results on the subbasin scale.

The results of both variables (ETA and SM) used in the cross-validation were moderate to very good in the catchment for both models. In summary both models performed equally during all steps of the evaluation procedure. A significant deterioration from EWEMBI to W5E5 was not found and most of the discrepancies in the water balance were present at parts of the headwater subbasins. Both models were able to capture the contrasting climate periods with slight reductions in the quality in dry or cold phases. No notable differences were determined in the cross-validation of the water balance components SM and ETA. All steps were successfully performed and passed.

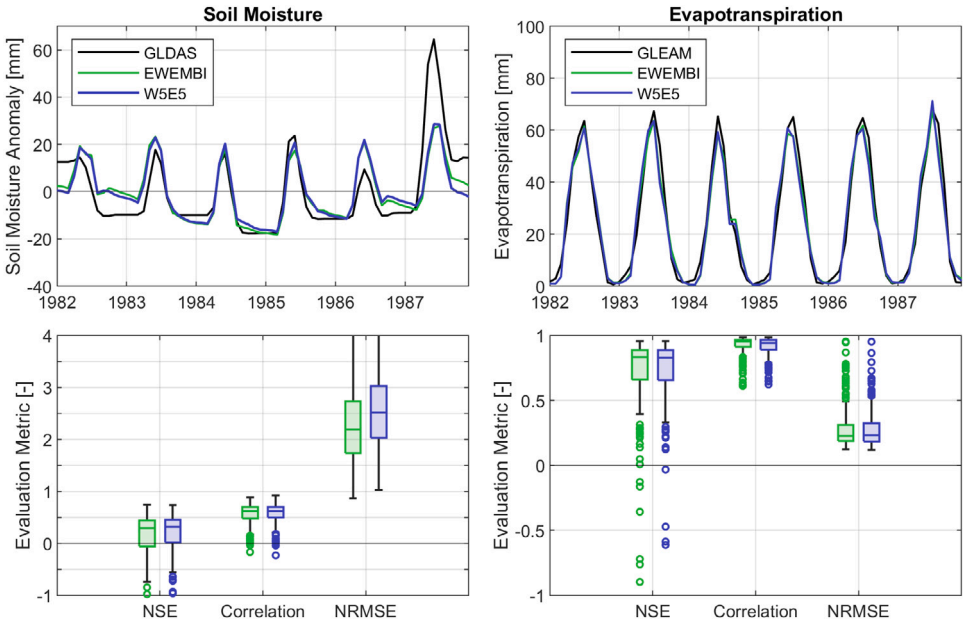

Fig. 4. Evapotranspiration and soil moisture performance in the period 1982–1987. The top panels shows the evapotranspiration and soil moisture estimates from SWAT compared to the results obtained from GLEAM and GLDAS, respectively, at the basin scale. The lower row demonstrates the subbasin performance of the SWAT models evaluated with the Nash–Sutcliffe Efficiency (NSE), Pearson correlation (r) and Normalized Root Mean Square Error (NRMSE) metrics for soil moisture and evapotranspiration. Outliers (outside 1.5 times the interquartile range above or below the upper/lower quartile) are indicated as green or blue dots, respectively. (For interpretation of the references to color in this figure legend, the reader is referred to the web version of this article.)

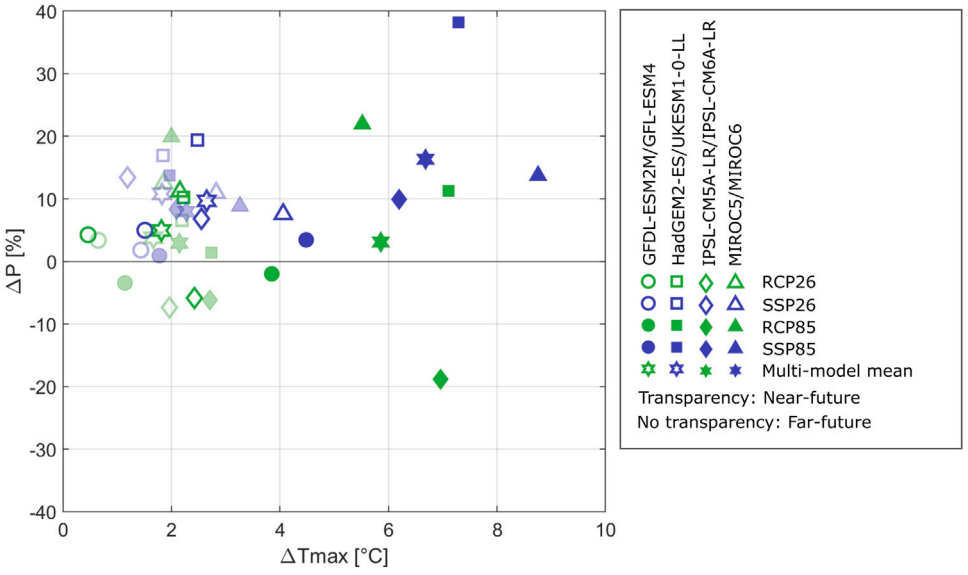

Fig. 5. Mean projected meteorological changes of $Tmax\&P$ for the near (2020–2049) and far (2070–2099) future periods, eight GCMs (four per ISIMIP phase), both scenarios and both ISIMIP phases compared to the baseline (1971–2000). $\Delta Tmax$ refers to the mean annual daily maximum temperature change. Analogously, ΔP corresponds to the mean annual precipitation change. Green — ISIMIP2, blue — ISIMIP3; filled/non-filled — high or low emission scenario; fill/outline transparency — near or far future; symbol — individual GCM (note, that the same symbol in green & blue indicates the respective predecessor/successor GCM. MMM refers to the multi-model mean in a specific period. (For interpretation of the references to color in this figure legend, the reader is referred to the web version of this article.)

3.2. Projected hydrometeorological changes of ISIMIP2b and ISIMIP3b

Results are separately presented for the meteorological forcings, the hydrological projections, the importance of the meteorological controls as well as the sensitivity analysis.

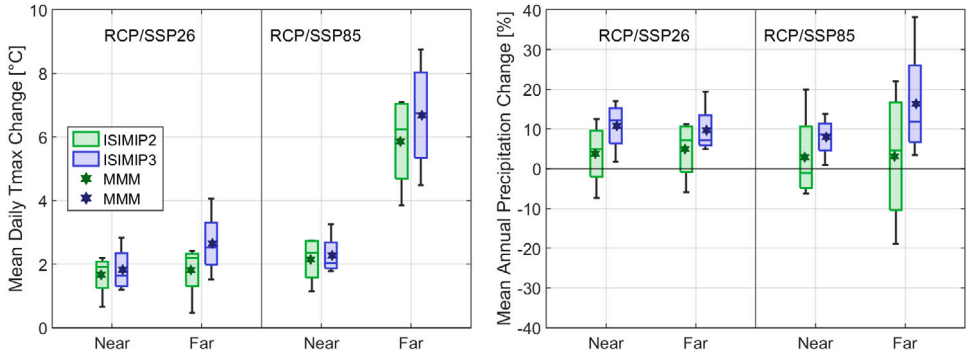

Fig. 6. Evaluation of mean projected temperature and precipitation changes compared to 1971–2000. Left panel: $\Delta Tmax$ change of both GCM generations, represented as multi-model mean (MMM), indicated by the hexagon and GCM spread (boxplot). Right panel: ΔP change with same illustration as for $\Delta Tmax$. Near — 2020–2049, Far — 2070–2099.

3.2.1. *Differences in meteorological forcing*

In the following we highlight the main differences of the two GCM generations with respect to the projected temperature and precipitation changes. Changes are represented as anomalies to the baseline for two future periods (see Section 2.5.1) under both scenarios. Temperature changes are evaluated as mean annual daily maximum temperature anomalies (from now on $\Delta Tmax$) rather than mean temperatures. Mean daily temperature changes are represented as proxy derived from $Tmax$. Precipitation changes ΔP refer to relative anomalies of the mean annual sum. Fig. 5 provides an overview of the meteorological projections of all scenarios, ISIMIP phases, GCMs and future periods.

The newer generation of GCMs produce generally higher temperatures as their former counterparts (comparison of equal blue and green symbols). In contrast to the high emission scenario, the temperature rise of an individual GCM between near and far future is weaker under the low emission scenario (same symbol, but different outline intensity). Under the low emission scenario the GCMs range from +1.5 °C to +4 °C temperature increase until 2099 under I3, compared to +0.46 °C to +2.4 °C under the old generation. Most GCMs scatter around +2 °C, without any significant difference between the two periods under RCP/SSP26. In contrast, under the high emission scenario the temperature rise ranges from +3.8 °C to +7.1 °C for RCP85, and 4.5 °C to 8.8 °C for SSP85. This underlines the higher climate sensitivity of the new generation of climate models in the study region. Comparing the warming rates in the far future on the GCM development level for the radiative forcing of 8.5 W/m^2, differences range from −0.77 °C (predecessor GCM computes higher temperatures) to +3.2 °C (successor GCM produces higher temperature). In average, the warming of the new climate models is around 0.82 °C higher in the far future period under the high emission scenario (MMM of +5.86 °C compared to MMM of 6.68 °C). The MMM of the low emission scenario for I2 is +1.82 °C and +2.65 °C for I3 in the far future period. Those results are in line with a generally higher climate sensitivity of CMIP6 GCMs compared to CMIP5 GCMs (Meehl et al., 2020).

Precipitation anomalies show a higher disagreement between both climate generations. Especially the old generation of GCM is characterized by diverging and contrasting precipitation patterns. In comparison, under I3 the GCMs consistently exhibit positive precipitation anomalies, albeit with strong deviations in their magnitudes. Under SSP85 in the far future period the projections range from +3.5% up to 38.2%, compared to −18.9% to 22% under RCP85. In general, the differences in magnitude between the near and far future for each GCM are less pronounced under RCP26/ SSP26, and more distinctive for RCP85/ SSP85, respectively. The projected change represented by the MMM is small under both RCP scenarios with values of +3.1% and +5% in the far future for RCP85 and RCP26, respectively. For the respective scenarios of I3 we observe an increase in precipitation of +9.7% (SSP26) and +16.3% (SSP85). In summary, the positive precipitation anomalies reflected by the various MMMs are enhanced under I3.

Besides, the inter-model range of I2 reveals a stronger spread (uncertainty) of precipitation anomalies for all future periods. The projected $\Delta Tmax$ anomalies present comparable inter-model ranges in all scenarios under I2 and I3 (Fig. 6). The discrepancy in the projected precipitation anomalies of the two generations arises mainly from specific regional contrasts, which are further addressed in the discussion section.

Moreover, deviations are found in the seasonal projections of precipitation. While both GCM families show an increase from October to May/June, they differ in late Summer and early Autumn. The MMM of the I3 ensemble does not significantly differ from the historical period in this period. However, in I2 the MMM shows strong declines of up to 30%. With respect to the seasonal patterns, all effects are more distinctive in the respective high-emission scenario and the far future period (See A1, A2).

3.2.2. *Hydrological impacts*

The hydrological models were forced with the meteorological inputs of the different GCMs and scenarios until 2099. However, due to differences in the time of departure from the historical to the projection period between the two GCM generations (2006 and 2015), different time series lengths were available for the trajectories. The impact models for I2 and I3 are based on the individual parameter sets from the respective reference datasets (EWEMBI or W5E5). Here, we present the results of the climate impact study on various hydrological components on the basin scale. Discharge results are thus presented for gauge Uchterek.

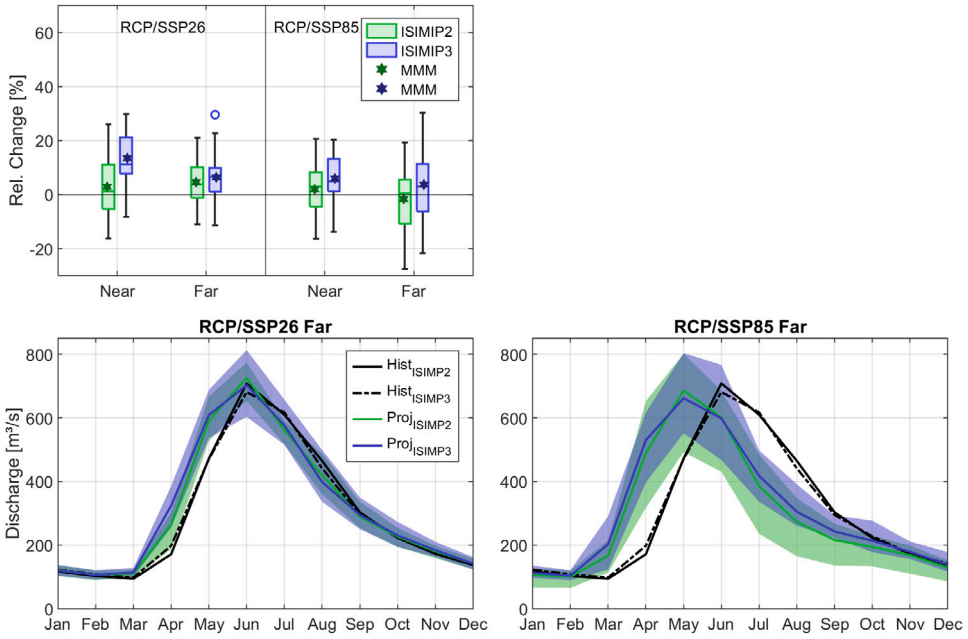

Fig. 7. Mean annual and long-term seasonal discharge projections at the basin outlet (Gauge Uchterek) compared to the historical period (1971–2000). Upper left panel: Mean annual projections and model spread for two different future periods for both GCM families and both scenarios. Bottom panels: Seasonal discharge projections for the far future period under RCP/SSP26 and RCP/SSP85. Near — 2020–2049, Far — 2070–2099.

Discharge. A summary of the results is provided in Fig. 7. In the far-future period the MMM of the annual mean flow is projected to change by +3.6% under SSP85 (+6.3% SSP26) and −0.7% under RCP85 (+5% RCP26). However, we observe significant seasonal shifts towards an earlier onset of the high flow period. Under the high emission scenario, peak flow is shifted by one month from June to May with a high agreement between the MMM of both, the I2 and I3-driven models for the far-future period. While Spring flow is projected to increase drastically under RCP26 (31.6%) and RCP85 (82.5%), Summer flow trajectories show significant decreases under the old generation of GCMs (−3.7% for RCP26 and −28.5% for RCP85). The I3-forced models exhibit similar patterns. Spring flow is projected to increase by 26.2% and 80.2%, respectively for SSP26 and SSP85 compared to a reduction of −2% (SSP26) and −24.4% (SSP85) in Summer.

The contrasting seasonal shifts in Spring and Summer have compensating effects with respect to annual mean flow changes. Despite an overall strong agreement in the seasonal MMM, both ISIMIP phases reveal differences regarding their uncertainties (see uncertainty bands in Fig. 7)). The agreement is detected in both scenarios in the far-future period. The uncertainties become larger with time and are more pronounced for the high emission scenarios. Besides, the lower boundary of the inter-model range is smaller under I2 in the high emission scenario (far-future) throughout the year.

Evapotranspiration. Stronger deviations between I2 and I3 are found in the ETA projections. Higher mean annual ETA anomalies are observed for I3 in both scenarios and both periods (expressed as MMM). We find a discrepancy of around 6% in the ensemble mean within the low emission scenario (Fig. 8) in the two periods. Under the high emission scenario the discrepancy between the I2 and I3-driven models increases with time. This leads to differences of 14% at the end of the century in the MMM (+9.32% I2 and +23.97% I3).

It becomes apparent that the reason is mainly due to negative Summer anomalies under RCP85 while the newer estimates are positive (−9% in MMM of I2 and +5% I3) for the far-future period. The effect is further amplified due to higher ETA estimates under SSP85 from March to June. The discrepancy of Summer ETA indicates differences in the available SM within this period (see also Fig. 9 lower right panel). The impact is likely to be induced by the deviations found in Summer precipitation of I2 and I3 (Fig. A2). For example in the far future period the relative ETA changes from June to September under RCP85 are −9.8% compared to a reduction of −27.5% in precipitation (model median). In the same period under SSP85 precipitation increases by +1.8% supported by an ETA raise of +4.8%, which is almost in balance. Similar patterns also occur under the low emission scenario, although not as distinct. The results are illustrated in Fig. 8.

Soil moisture. Fig. 9 illustrates the projected SM changes in the Naryn Basin. Both, I2 and I3 projections agree in their overall tendency of a significant decline in SM under all scenarios and periods. However, discrepancies are found in the uncertainties and magnitudes of the detected patterns. The projections of the older GCM family constitute larger uncertainties with less negative seasonal anomalies in the far-future period in the low emission scenario. In contrast, the negative seasonal anomalies in the high emission scenario are more pronounced than for I3. In particular, Summer and early Autumn are characterized by a significant

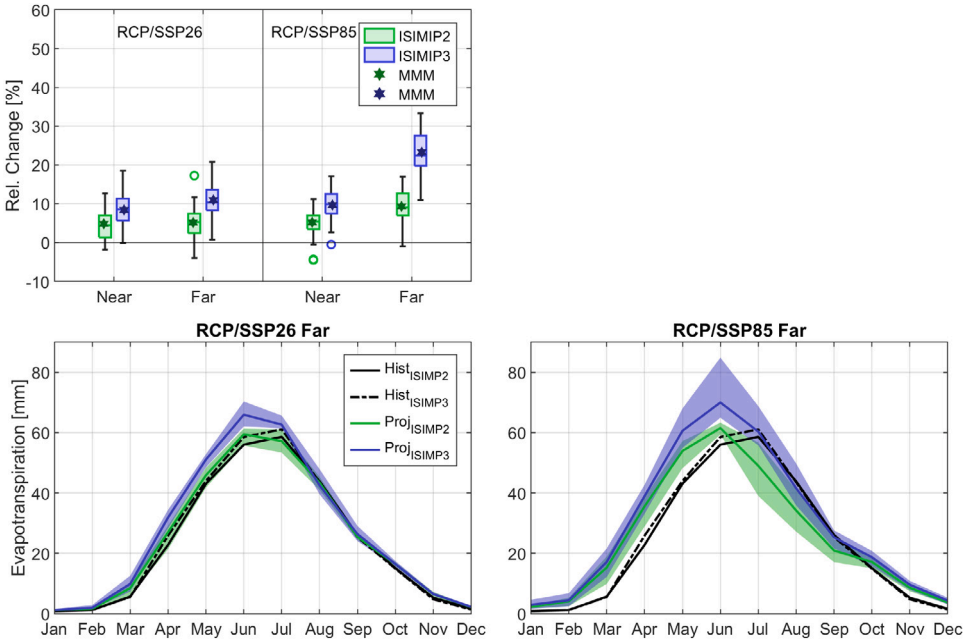

Fig. 8. Mean annual and long-term seasonal actual evapotranspiration (ETA) projections at the basin scale. The panels information are identical to Fig. 7.

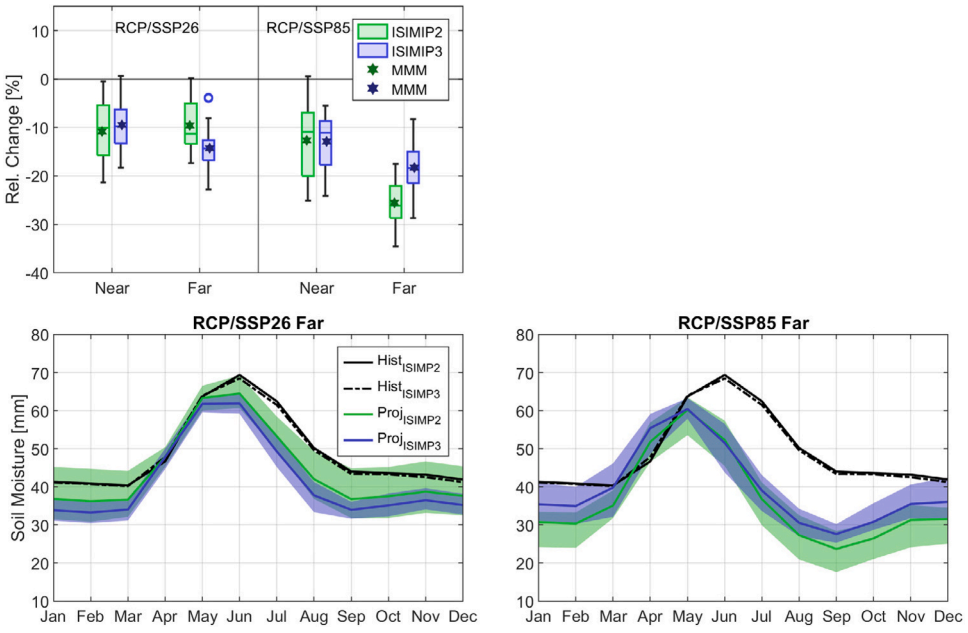

Fig. 9. Mean annual and long-term seasonal soil moisture (SM) projections at the basin scale. The panels information are identical to Fig. 7.

decline in the MMM in all periods and scenarios under both climate model phases. For SSP85, available Summer SM is projected to decrease around −33% (far-future) which is in line with a decrease of −36% for RCP85. In the low emission scenario (again far-future) Summer SM projections reveal a decrease of −17% and −12% for SSP26 and RCP26, respectively. Similar reductions for the far-future are observed in Autumn, with MMM SM decreasing by −27% under SSP85, −38% under RCP85, −18% under SSP26 and -14% for RCP26. Positive SM anomalies are detected in April under both ISIMIP generations in the high emission scenario and far-future period (+11% MMM of RCP85 and +15.8% MMM of SSP85).

Annual SM anomalies under RCP26 remain relatively constant from near to far-future (around −10% in MMM), while a marked decline under SSP26 is found (from −9.5% to −14.3%). In the high emission scenario, the MMM of both, the I2 and I3-driven models

project a negative SM anomaly of −13% in the Near-future. For the far-future an even more distinct SM decline of −18% under SSP85 and −26% under RCP85 is detected, respectively. Besides, the lower boundary of the SM projections under RCP85 is −35% (around −29% for SSP85). The lower reductions under SSP85 are in line with the significant precipitation rise (see Fig. 6) compared to the I2-derived counterpart.

3.3. Meteorological controls of the soil moisture and evapotranspiration feedback

A PC system was established to evaluate the relevance of meteorological changes on the SM-ETA feedback and to determine differences in the feedback between I2 and I3. As the basin is generally water-limited, SM anomalies control ETA anomalies (positive relationship), while in energy-limited regions the coupling would be reversed and ETA anomalies would lead to SM variations (negative relationship) (Berg and Sheffield, 2019). For this reason, we calculated the PC between ETA and SM, rather than ETA and precipitation (which might be suitable as SM proxy). Monthly anomalies of the MMM for the two periods AMJ and JAS were used for the evaluation. The two periods together comprise the vegetative season. Due to hydrometeorological differences within the vegetative season, the season was split to identify potential contrasting patterns. The PC results are supported by standard Pearson Correlation values in order to highlight the magnitude of confounding effects.

The results of the PC analysis are illustrated in Fig. 10, where the upper four panels refer to the period from May to June and the lower four to June to September. In the AMJ period a strong positive relationship between temperature and ETA is found for the near-future within all scenarios under both ISIMIP phases. Here the effects of precipitation and SM are small (gray crosses versus colored bars), which indicates a sufficient water availability in this period in the near-future to cover the ETA demand. This is in agreement with the constant to slight increase in precipitation in these months (Fig. A2). Vice versa, the SM control on ETA in the near-future of the AMJ period is rather small (< 0.5), albeit higher under I2 which is confirmed by higher precipitation projections causing a slightly higher water availability under I3 (Fig. A2). Confounding effects in the ETA control are relatively weak and most pronounced in the SSP26 near-future relationship of SM and ETA. The ETA variance is therefore explained to a large degree of temperature and precipitation. We can already see a strong decline of the importance of temperature on ETA anomalies under the high emission scenario in the far future (I2 and I3). This implies an increase in the positive SM-ETA coupling and a potential stressor for soil water. A cross-validation with Fig. 9 shows that this mostly refers to June where soil decussation under RCP and SSP85 is substantial in the far future. In contrast to I3 the I2 projections of RCP85 the SM-ETA feedback increases significantly while under SSP85 the relationship of temperature and SM with ETA are close with small PC values (< 0.5). Under the low emission scenario (far future) ETA variations are still controlled mainly by temperature, with PC magnitudes similar to the near future under I2 and I3.

The AMJ period coincides with the rainy season and the PC values of temperature and SM are predominantly weaker as for ETA. Nearly all PCs of temperature and SM are below 0.5 (all scenarios, periods and both ISIMIP phases) or even below 0.25. Under I2 no strong changes in the behavior of SM and temperature are found between near and far future (both scenarios). A similar development is shown under I3. However, the contra-intuitive positive association of temperature and SM is largely mitigated by the fact that the strengths of the relationships are insignificant and the signs heterogeneous. In the high emission scenario of I3 water-limitation becomes more apparent through a negative relationship (although weak) between SM and temperature in the far future. This is in accordance with the SM-ETA coupling in the AMJ period, where the T-ETA association is substantially decreased and SM becomes more important in the far future.

The generally drier JAS season is characterized by SM shortcomings and pronounced water-limited conditions. This is also reflected in the PC values of the JAS season. The SM-ETA feedback is strongly positively correlated in the near and far future of all scenarios under I2 and I3. The actual Pearson correlations between temperature and ETA show strong negative relationships, which would imply the unintuitive fact that rising temperatures are associated with a decline in ETA (again all scenarios of I2 and I3 and far and near future). However, most of the variance can be explained by the effects of precipitation and SM. Hence, the corresponding PCs of temperature and ETA are much weaker in absolute values than the Pearson correlations. For the I2 cases and the near future of the SSP85 the negative behavior is even reversed (positive sign of PC). While under both I2 scenarios the dominant SM control of ETA anomalies remains constant from near to far future, the positive feedback is marginally reduced from near to far future in the I3 counterparts. This is especially in line with the precipitation projections in the JAS period of the high emission scenarios, which have a significant drop under I2 compared to I3 and is also visible in the SM anomalies of the high emission (Figs. 9 and A2). The advanced water limitation under I2 compared to I3 is clearly visible in the corresponding PC values. Generally the higher the PC value of SM-ETA, the stronger the feedback and the more distinctive the water limitation. Accordingly, two entirely contrasting pictures can be revealed in the control of ETA variations.

The explanation of SM anomalies is again more ambiguous. For the high emission scenarios (I2 and I3) of the near future a substantial portion is explained by temperature anomalies. Both show a strong negative relationship indicating a strong SM decrease with rising temperatures. The negative relationship is also present in the far future (both scenarios) as well as the low emission scenarios of the near future, yet not as notable (< 0.5). For the near future of the low emission scenarios the missing strength is attributed to the smaller positive temperature anomalies compared to the high emission scenarios. The reduced dominance of temperature in the far future is probably caused by an already advanced desiccation of soils (water limitation higher as in near future). The selection of ETA as one of the confounding variables for SM might be doubtful, since SM controls ETA and not vice versa. At least it becomes apparent that the confounding effects under I3 here are relatively high. Fig. A4 provides an additional example of sensitivities of multiple variables to annual temperature anomalies.

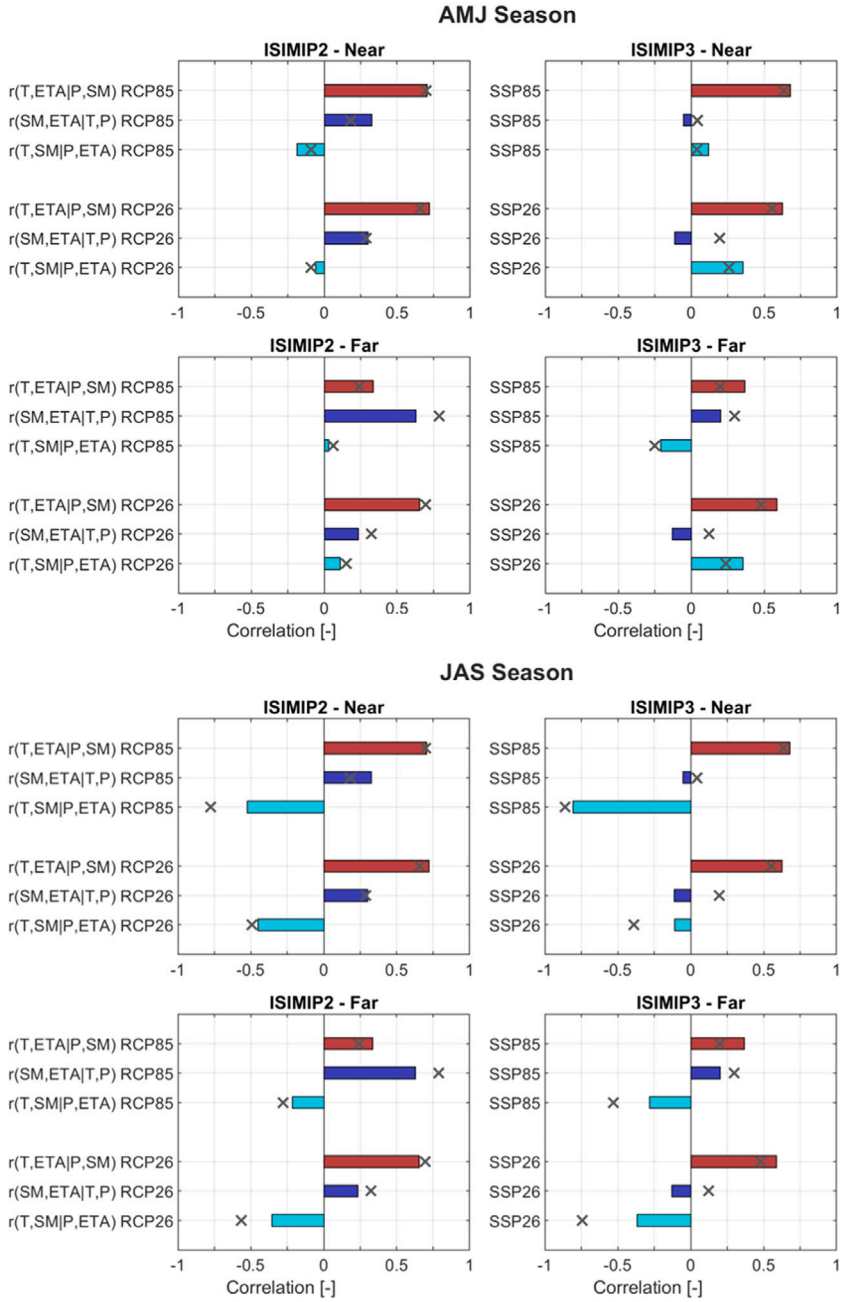

Fig. 10. Relationship of monthly SM and ETA anomalies with temperature (T) or soil moisture (SM) anomalies for the two ISIMIP phases and two scenarios during the two periods April to June (AMJ) and July to September (JAS), which together represent the vegetation season. Shown in red, partial correlation of ETA and T while controlling for P and SM. Shown in blue, partial correlation of ETA and SM while controlling for T and P. Shown in cyan, partial correlation of SM and T while controlling for ETA and P. Gray crosses indicate the corresponding Pearson correlation coefficients. $r(T, SM|P, ETA)$ indicates the PC between T and SM controlling for P and ETA. (For interpretation of the references to color in this figure legend, the reader is referred to the web version of this article.)

4. Discussion

In this study, we investigated how climate impact assessment agrees and diverges under a subset of I2 and I3 GCMs. To produce a reliable and robust hydrological model for the impact assessment we followed the recommendations proposed by Krysanova et al. (2018, 2020).

4.1. Evaluation test

The evaluation procedure produced meaningful and comparable results for both, the SWAT model forced with EWEMBI as well as with W5E5. All steps of the evaluation procedure were successfully passed and the models performed satisfactorily to well in most cases under contrasting climate periods, on multiple temporal scales, for various GOF criteria as well as for ETA and SM in addition to discharge. In detail, however, there were differences at the subbasin level, where individual gauges showed a poorer performance than for example at the basin outlet. Thus, two similar parameter sets were identified for both reference datasets serving as base for the impact assessment. GOF results were on average around 0.75 for NSE, 0.82 for KGE and 9.4% for PBIAS in the basin (considering all gauges). Moreover, warm and wet periods were better reflected (NSE_{wet} 0.8, NSE_{warm} 0.75) than cold and dry periods (NSE_{cold} 0.71, NSE_{dry} 0.70). Similar difficulties and weaker model performances are for example also reported in Vaze et al. (2010) for a catchment in Australia.

However, due to the crucial role of nivo-glacial processes in CA catchments, more emphasize should be placed on these processes in future studies. E.g. considering snow cover as in Hofmeister et al. (2022), glacier mass balance as Wortmann et al. (2018) did or snow water equivalent data (see Tuo et al. 2018) in the calibration process, if available, could produce an even more consistent and reliable picture of the system. Deficiencies were mostly observed in the high-elevated headwater part (see Tables 2 and 3), where NSE values were in average only around 0.6. These are mainly due to model weaknesses with regard to the representation of glaciers. We therefore agree with Saks et al. (2022) that future studies should consider these aspects and evaluate expected peak flow more closely.

It must also be mentioned that the approach followed here logically does not necessarily guarantee that the robustness of the model adequately reflects all projected changes. This is particularly the case for the contrasting climatological periods, since rates of change are likely to be more pronounced in the future on the one hand, and on the other hand the relatively short historical period (restricted due to data availability) may not adequately reflect the influence of persistent changes over a longer period of time. these deviations and assumptions that might be only partially representative are described in detail in Stephens et al. (2020).

4.2. Meteorological changes

Projected temperature raises agree throughout the year in all periods under the new and old generation of GCMs. In contrast, precipitation disparities have shown to be one of the major differences between I2 and I3. While precipitation changes observed under I2 are mostly in line with other related studies (Lutz et al., 2014; Luo et al., 2018; Huang et al., 2014), the higher increase under I3 has not yet been comprehensively and extensively addressed in the literature. The same applies to the associated effects on the hydrological cycle. Discrepancies in the precipitation projections between I2 and I3 arise mainly from regional contrasts in the basin. Under SSP26 and SSP85 a continuous rise throughout the whole basin is projected, with a marked characteristic in the Kekerim subbasin. I2 contains two counteracting patterns, the Western part of the basin receives more precipitation, which is amplified in the high emission scenario, while on the other hand the Eastern (and headwater) part is characterized by a decline in precipitation. The decline is also even more significant in the high emission scenario and for the far future period.

We provide a first estimate of hydrological impacts triggered by precipitation changes under both ISIMIP generations. The deviations in projected precipitation anomalies (consistent positive precipitation anomalies with MMM of +16.3% under SSP85 compared to +3.1% under RCP85 in the far-future) come along with a higher climate sensitivity in the new ensemble of climate models (warming rate in average +0.82 °C higher until 2100 in high emission scenario). However, a lot of the current research focuses on the higher climate sensitivity of CMIP6 models including the potential or necessity to constrain warming trends of models that tend to be on the upper edge (Tokarska et al., 2020; Sherwood et al., 2020). As only a subset of GCMs was available and included, future studies might extend the efforts with a larger sample.

Further, although projects like ISIMIP add a huge value for climate impact studies the generally coarse resolution of the GCMs might not be suitable for all studies and regions. Especially for small basins the resolution could be insufficient. Hydrological scale patterns could be missed, this problem might also affect the higher elevated parts of the study area, where the performance of the models (for all variables) was deteriorated. Meteorological processes of individual mountain ranges might be inaccurately represented. However, data limitations make it difficult to evaluate this thesis in detail. In any case, we assume that Regional Climate Models are favorable and would add value to future studies if possible to include.

We also would like to at least mention that (depending on the methodology and data availability) an assessment of the GCM performance might be reasonable in advance of the actual study to for example exclude poor-performing climate models or to take into account a weighting approach to reduce their importance within the results. If for some reasons GCMs are not applicable in a study, we would also like to emphasize to consider perturbations of the observed climatology to draw conclusions of the future hydrology based on these synthetic time series. Examples can for example be found in Rasouli et al. (2019b,a)

4.3. Hydrological changes

The projected MMM of all hydrological variables generally agree between I2 and I3 on the annual and seasonal scale. MMM discharge projections were similar across both ISIMIP phases. They showed a significant shift in the flow regime. Peak discharge is projected to occur one month earlier (June to May) under the high emission scenarios by the end of the century. This is consistent with what was reported by other authors (Gan et al., 2015; Didovets et al., 2021). The shift is mainly driven by substantial increases in Spring snowmelt followed by a strong decline in Summer A3. The summer deficit agrees with the water shortage found for

SM. Summer deficits of discharge and SM could cause and promote water stress in the region. This is particularly evident since summer water availability directly affects irrigation demand during the vegetative season and water storage for energy production. Especially for higher projected temperatures and thus an increase in potential evapotranspiration estimates, future water demand could significantly rise and constitute an additional stressor.

Moderate deviations were found in the ETA trajectories, with stronger increases projected under I3 (difference of 6% in MMM of I2 and I3 in low emission scenario and 14% in high emission scenario at the end of the century). The higher estimates are likely to be triggered by a combination of higher projected temperatures (higher energy-availability, Fig. 6) as well as weaker SM reductions (higher water-availability, Fig. 9). ETA increases referred mainly to the first half of the year, the period where the most significant precipitation increases were observed. The period was also characterized by a strong increase in snowmelt (Fig. A3), an additional source of water. The described impacts are more pronounced under the high emission scenario and the far-future. The ETA trajectories are consistent with recently reported trends for CA and globally. And the impacts could significantly contribute to future desertification, one of the major risks in CA (Huang et al., 2020b; Ma et al., 2021).

Notable SM deficits in Summer (−36% in MMM of RCP85 and −33% under SSP85 in the far-future) and Autumn (−38% in MMM of RCP85 and −27% under SSP85 in the far-future) were projected for both GCM generations, which could act as potential stressor for the agricultural productivity. Summer and Autumn SM deficits could thus induce and promote future agricultural droughts. Droughts that promote land degradation are already present in CA (Zhang et al., 2018). According to our results, indications of negative changes in the vegetation dynamics, caused by soil moisture deficits, which became particularly pronounced after the 90's (Li et al., 2015; Deng and Chen, 2017), could thus also represent a substantial future risk in the basin. The crucial role of SM for drying in CA is also illustrated in Hu et al. (2018), who used a correlation analysis to demonstrate the importance of SM. Although most of the studies available focus on whole CA, solely on the historical period or use related variables such as NDVI (or variants of it) and total water storage (Jiang et al., 2017; Xing et al., 2022; Zhou et al., 2015; Peng et al., 2021), our study supports to assess these future risks at the local level. The negative anomalies were slightly smaller under I3 due to an attenuation caused by a raise in precipitation (annual decrease in MMM of −18% for SSP85 and −26% for RCP85 in the far-future). Annual SM shortcomings tend to be stronger for I3 under the low emission scenario and smaller under the high emission scenario compared to I2 by end of the century. Summarized, the findings indicate the vulnerability of the region to SM shortages.

Our PC results provide evidence that shifts in the role of the meteorological drivers can be expected from near to far future as well as between I2 and I3 in both periods (AMJ and JAS). This leads to partly significant deviations and changes in the SM-ETA coupling (from near to far under both GCM generations as well as between them and in both seasons). We find clear differences in the strength of the SM-ETA relationship in the two seasons AMJ and JAS, where the latter is considerably more water-limited. While under I2 the pressure on soil moisture, reflected in the strong control of ETA, remains relatively constant from near to far future (both scenarios), we see a attenuation of the strongly positive relationship under I3 (both scenarios) from near to far. This development represents the different precipitation trajectories, where the I3 JAS rainfall does not show the drop which is especially visible in the RCP85 and thus likely leads to a mitigated negative SM evolution under I3, albeit still severe. The strong water limitations in JAS are expected to exacerbate the pressure on water resources to meet the demand. The resulting implications for example on land degradation or the occurrence of droughts are similar to those mentioned already above. However, the PC results underline the assumption of a reinforced SM-ETA coupling under both generations of climate models, yet with a marginal shift towards less water-limitation under I2 in JAS. The strength of the SM-ETA coupling could be seen as indicator for vegetation conditions (Ibrahim et al., 2015) and in terms of a positive coupling reduced moisture availability (Berg and Sheffield, 2019). The strong positive future relationship between the two variables in the basin is also in accordance what is expected roughly on the global scale, when analyzing GCM outputs (Berg and Sheffield, 2018; Berg et al., 2015; Dirmeyer et al., 2013). A limitation which applies not only to our study but to many hydrological impact studies are missing atmospheric feedbacks which are connected to the ETA-SM coupling, such as evaporative cooling.

For the generally wetter AMJ season we can already identify a positive increase in the SM-ETA relationship under I2 and I3 from near to far future, particularly in the high emission scenarios. This provides evidence that the water-limited regime could further advance in the region, despite precipitation projection in the far future tend to be positive for I2 as well as I3. In other words, the importance of SM variations to explain ETA variations increases. This shift in the future importance of SM is enhanced by the decreasing dominance of temperature to explain ETA variations under the high emission scenarios. One major deviation between I2 and I3 is found in the magnitude of the SM-ETA feedback in the far future of the high emission scenarios. Under RCP85 the explanatory power of SM replaces the one of temperature as major controlling factor. In contrast, although the importance of SM increases with a simultaneous decline of temperature the final magnitudes in the far future are relatively close to each other (with small values < 0.5). We assume that this is caused by the slightly larger increase in precipitation under I3 in AMJ attenuating the increased demand of rising temperatures. However, it is expected that further increasing temperatures would also tip the relationship and approach the conditions of I2.

Stationarity was assumed for the vegetation season, which was used for comparability reasons, although the period can vary with land use (and thus in space) (Zhang et al., 2018; Zhou et al., 2015). As the climatic shifts are likely to shift the vegetative season as well, a constant period represents a simplified manner.

We only included one hydrological model in the assessment. An ensemble of impact models would further improve the robustness of the results. Structural differences in impact models can result in significant deviations in the projections and identify adequateness or inadequacy of impact models for different conditions (Kundzewicz et al., 2018; Wen et al., 2020; Su et al., 2016). Also land use changes were neglected, which are likely to affect processes such as runoff generation, albedo-associated mechanisms or translation and retention.

5. Conclusions

Our study shows that despite advances in the forcings of impact models, as a result of GCM, scenario or bias-adjustment developments, estimated impacts are in general concordance.

These are particularly evident in the projected shifts of the hydrological regime and a sharp increase in soil desiccation. We find a shift in peak flow of one month due to an earlier start of the melt season in the high emission scenarios. The earlier onset leads to an increase in discharge in Spring followed by a decline in Summer. Across both GCM generations and all scenarios, the impact assessment further indicates substantial soil moisture deficits, especially in Summer and Autumn.

However, disagreement between I2 and I3 is found in the evapotranspiration estimates, which are higher in the new generation. Temperature projections of I3 are consistent with the general recognition of being warmer than under previous generations (higher climate sensitivity). Rather large deviation between the two generations are found in the precipitation projections. Although consistently positive precipitation anomalies are observed under I3, the projected SM deficits are substantial under both phases, indicating the region's vulnerability. This underlines the sensitive interplay between the different components precipitation, soil moisture and evapotranspiration.

Deviations in the temperature and precipitation projections of I2 and I3 in the two examined seasons (AMJ and JAS) reveal significant effects on the SM-ETA coupling in the basin. Expressed as PCs we find enhanced water-limited conditions in the AMJ season at the end of the century, particularly in the high emission scenarios. The advanced importance of SM is directly shown as increase in the positive relationship between SM and ETA and indirectly through the decrease in the dominance of temperature on ETA. The inherently drier JAS season with its strong positive SM-ETA coupling remains constant under the near and far future of I2, while there is a slight decrease with time under the corresponding I3 scenarios. This indicates that the general and progressive water-limitation among both ISIMIP generations could be at least slightly weakened under I3, albeit it is still intense. Differences in the magnitudes of effects between I2 and I3 are likely to be caused by mitigating effects present under I3, mostly referred to positive or at least constant precipitation trajectories in the vegetative season.

CRediT authorship contribution statement

Timo Schaffhauser: Conceptualization, Methodology, Writing – original draft, Visualization, Methodology, Formal analysis, Software, Writing – review & editing, Data curation. **Stefan Lange:** Data curation, Methodology, Resources, Writing – review & editing. **Ye Tuo:** Conceptualization, Methodology, Writing – review & editing. **Markus Disse:** Funding acquisition, Conceptualization, Resources, Writing – review & editing.

Declaration of competing interest

The authors declare that they have no known competing financial interests or personal relationships that could have appeared to influence the work reported in this paper.

Data availability

Data will be made available on request.

Acknowledgments

We want to thank the ISIMIP project in which context the guideline for the evaluation test for impact studies was created, as well as for providing us the necessary data for our study. In addition we want to thank the German Research Centre for Geoscience for sharing observational data with us, without which it would not have been possible to conduct our study and Florian Betz for his critical discussions and regional expertise. The authors from TUM also want to thank the BMBF (Bundesministerium für Bildung und Forschung) for the funding of the "OekoFlussPlan" project (grant number 01LZ1802B).

Appendix A

A1

Table A.1
Overview of the model parameters used in the calibration of the hydrological models driven by the reference datasets of the two ISIMIP families, namely EWEMBI and W5E5. Parameter ranges were individually set and fixed for each calibrated subbasin/gauge.

Category	Parameter	File	Description
Water balance	PLAPS	.sub	Precipitation Lapse Rate [mm/km]
	TLAPS	.sub	Temperature Lapse Rate [°C/km]
Snow	TIMP	.sno	Snowpack Temperature Lag Factor [-]
	SMFMX	.sno	Melt Factor for Snow on 21st June [mm H_20/(°C*d)]
	SMFMN	.sno	Melt Factor for Snow on 21st December [mm H_20/(°C*d)]
	SMTMP	.sno	Snowmelt Temperature [°C]
	SFTMP	.sno	Snowfall Temperature [°C]
Groundwater	ALPHA_BF	.gw	Baseflow Alpha Factor [days]
	GWQMN	.gw	Shallow Aquifer Threshold for Baseflow to Occur [mm]
	GW_DELAY	.gw	Groundwater Delay [days]
	RCHRG_DP	.gw	Fraction of Percolation for Deep Aquifer [-]
	REVAPMN	.gw	Shallow Aquifer Threshold for Revap to occur [mm]
ETP & Runoff	EPCO	.hru	Plant Uptake Compensation Factor [-]
	ESCO	.hru	Soil Evaporation Compensation Factor [-]
	SURLAG	.hru	Surface Runoff Lag Time [days]
	CN2	.mgt	Curve Number for Moisture Condition II [-]
Soil	SOL_AWC	.sol	Available Water Capacity for the Soil Layer [-]
	SOL_k	.sol	Available Water Capacity for the Soil Layer [mm/h]
	SOL_BD	.sol	Soil Bulk Density [mg/m^3]

A2

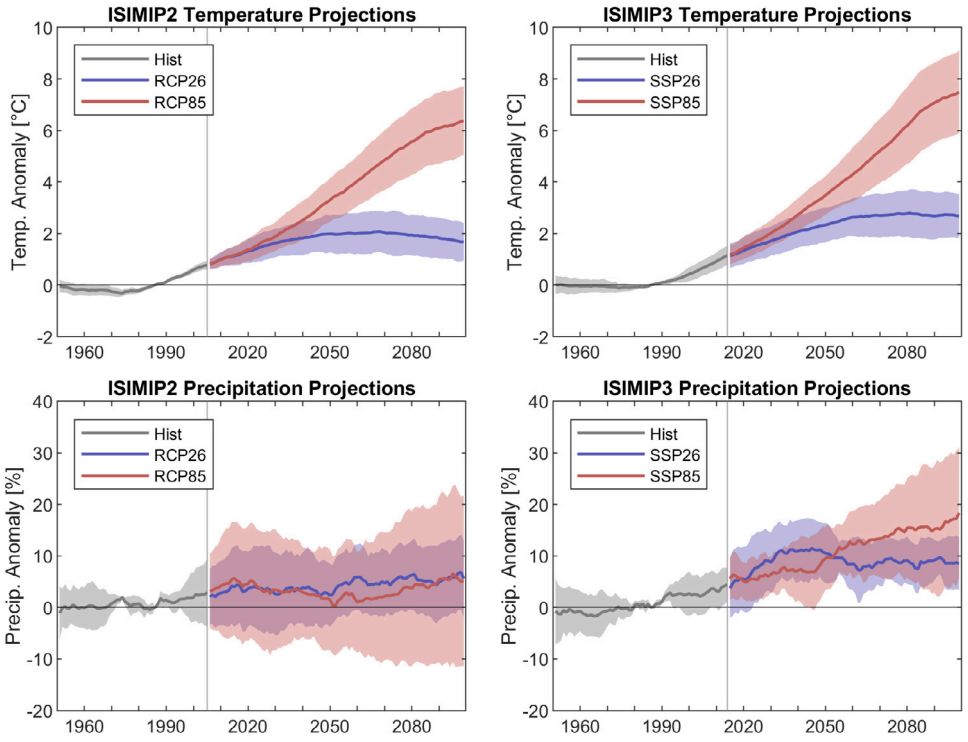

Fig. A1. Temperature and precipitation trajectories at the basin scale for the high and low emission scenarios of ISIMIP2 and ISIMIP3 until 2099. The shaded area refers to the standard deviation of the inter-model range. The straight lines represent the MMM. The historical period is indicated as gray.

A3

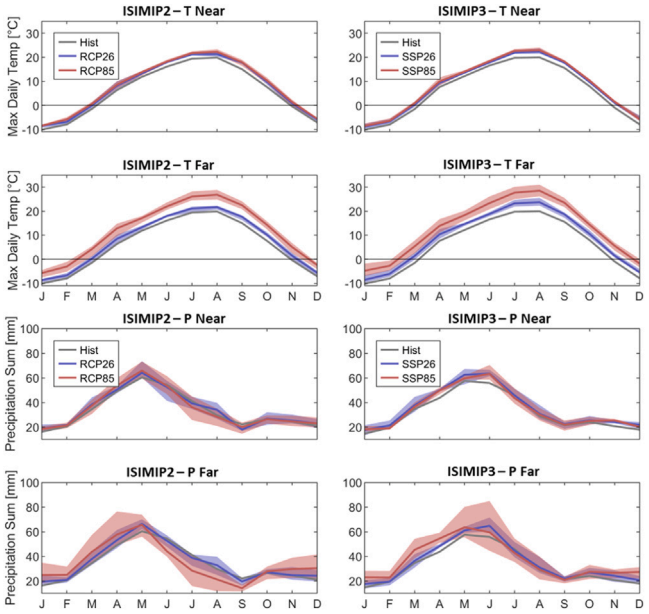

Fig. A2. Seasonal temperature and precipitation trajectories at the basin scale for the high and low emission scenarios of ISIMIP2 and ISIMIP3 for the near and far future period. The shaded area refers to the standard deviation of the inter-model range. The straight lines represent the MMM. The historical period is indicated as gray. P refers to precipitation and T refers to temperature.

A4

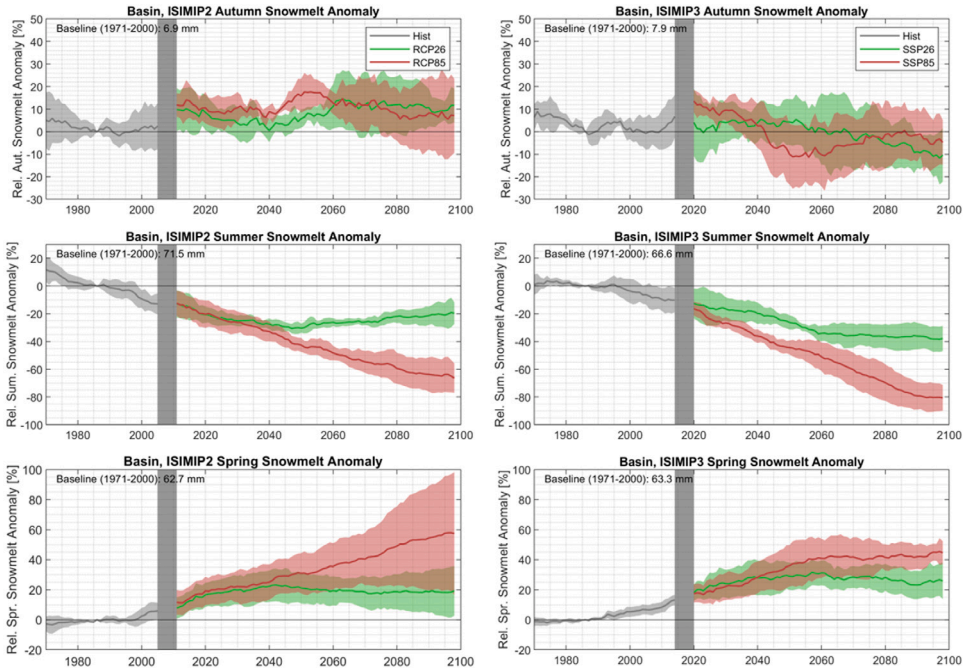

Fig. A3. Seasonal snowmelt projections under ISIMIP2 and ISIMIP3. The meteorological seasons are averages of: Spring — March, April, May; Summer — JJA; Autumn — SON. The vertical gray bar indicates the warm-up season required in the hydrological model, where no data is available.

A5

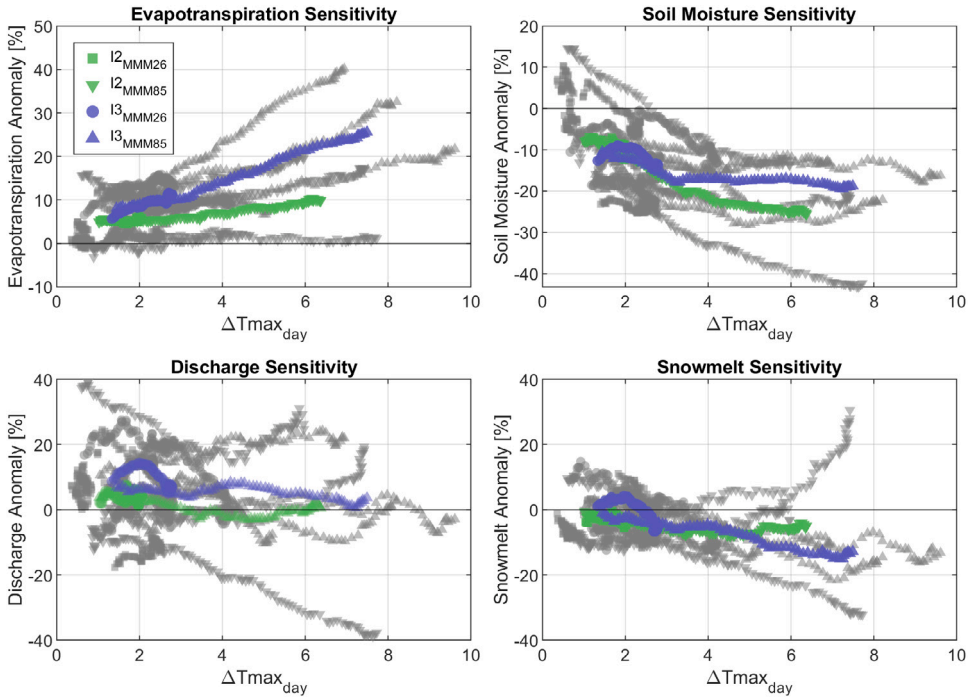

Fig. A4. Sensitivity of evapotranspiration, soil moisture, discharge and snowmelt to temperature variations under ISIMIP2 and ISIMIP3. Sensitivities are assessed for projected annual anomalies of each variables and the respective projected temperature change. I2 refers to ISIMIP2 and I3 to ISIMIP3. Gray markers correspond to the individual GCM results, color symbols represent the multi-model mean (MMM). Results consider all projected values. (For interpretation of the references to color in this figure legend, the reader is referred to the web version of this article.)

References

Aizen, V.B., Aizen, E.M., Melack, J.M., 1995. Climate, snow cover, glaciers, and runoff in the tien shan, central asia. J. Am. Water Resour. Assoc. 31 (6), 1113–1129. http://dx.doi.org/10.1111/j.1752-1688.1995.tb03426.x.

Arnold, J.G., Fohrer, N., 2005. SWAT2000: current capabilities and research opportunities in applied watershed modelling. Hydrol. Process. 19 (3), 563–572. http://dx.doi.org/10.1002/hyp.5611.

Arnold, J.G., Srinivasan, R., Muttiah, R.S., Williams, J.R., 1998. Large area hydrologic modeling and assessment part i: model development. J. Am. Water Resour. Assoc. 34 (1), 73–89. http://dx.doi.org/10.1111/j.1752-1688.1998.tb05961.x.

Barandun, M., Fiddes, J., Scherler, M., Mathys, T., Saks, T., Petrakov, D., Hoelzle, M., 2020. The state and future of the cryosphere in central Asia. Water Secur. 11, 100072. http://dx.doi.org/10.1016/j.wasec.2020.100072.

Barandun, M., Pohl, E., Naegeli, K., McNabb, R., Huss, M., Berthier, E., Saks, T., Hoelzle, M., 2021. Hot spots of glacier mass balance variability in central Asia. Geophys. Res. Lett. 48 (11), http://dx.doi.org/10.1029/2020gl092084.

Berg, A., Lintner, B.R., Findell, K., Seneviratne, S.I., van den Hurk, B., Ducharne, A., Chéruy, F., Hagemann, S., Lawrence, D.M., Malyshev, S., Meier, A., Gentine, P., 2015. Interannual coupling between summertime surface temperature and precipitation over land: Processes and implications for climate change. J. Clim. 28 (3), 1308–1328. http://dx.doi.org/10.1175/jcli-d-14-00324.1.

Berg, A., Sheffield, J., 2018. Soil moisture-evapotranspiration coupling in CMIP5 models: Relationship with simulated climate and projections. J. Clim. 31 (12), 4865–4878. http://dx.doi.org/10.1175/jcli-d-17-0757.1.

Berg, A., Sheffield, J., 2019. Historic and projected changes in coupling between soil moisture and evapotranspiration (ET) in CMIP5 models confounded by the role of different ET components. J. Geophys. Res.: Atmos. 124 (11), 5791–5806. http://dx.doi.org/10.1029/2018jd029807.

Bernauer, T., Siegfried, T., 2012. Climate change and international water conflict in central Asia. J. Peace Res. 49 (1), 227–239. http://dx.doi.org/10.1177/0022343311425843.

Berndtsson, R., Tussupova, K., 2020. The future of water management in central Asia. Water 12 (8), 2241. http://dx.doi.org/10.3390/w12082241.

Bosshard, T., Carambia, M., Goergen, K., Kotlarski, S., Krahe, P., Zappa, M., Schär, C., 2013. Quantifying uncertainty sources in an ensemble of hydrological climate-impact projections. Water Resour. Res. 49 (3), 1523–1536. http://dx.doi.org/10.1029/2011wr011533.

Changkun, M., Sun, L., Liu, S., Shao, M., Luo, Y., 2015. Impact of climate change on the streamflow in the glacierized chu river basin, central Asia. J. Arid Land 7 (4), 501–513. http://dx.doi.org/10.1007/s40333-015-0041-0.

Chen, Y., Li, W., Fang, G., Li, Z., 2016. Hydrological modeling in glacierized catchments of central Asia: status and challenges. http://dx.doi.org/10.5194/hess-2016-325.

Cucchi, M., Weedon, G.P., Amici, A., Bellouin, N., Lange, S., Schmied, H.M., Hersbach, H., Buontempo, C., 2020. WFDE5: bias-adjusted ERA5 reanalysis data for impact studies. Earth Syst. Sci. Data 12 (3), 2097–2120. http://dx.doi.org/10.5194/essd-12-2097-2020.

Dembélé, M., Hrachowitz, M., Savenije, H.H.G., Mariéthoz, G., Schaefli, B., 2020. Improving the predictive skill of a distributed hydrological model by calibration on spatial patterns with multiple satellite data sets. 56, http://dx.doi.org/10.1029/2019wr026085.

Deng, H., Chen, Y., 2017. Influences of recent climate change and human activities on water storage variations in central Asia. J. Hydrol. 544, 46–57. http://dx.doi.org/10.1016/j.jhydrol.2016.11.006.

Didovets, I., Lobanova, A., Krysanova, V., Menz, C., Babagalieva, Z., Nurbatsina, A., Gavrilenko, N., Khamidov, V., Umirbekov, A., Qodirov, S., Muhyyew, D., Hattermann, F.F., 2021. Central Asian rivers under climate change: Impacts assessment in eight representative catchments. J. Hydrol.: Regional Stud. 34, 100779. http://dx.doi.org/10.1016/j.ejrh.2021.100779.

Dirmeyer, P.A., Jin, Y., Singh, B., Yan, X., 2013. Trends in land-atmosphere interactions from CMIP5 simulations. J. Hydrometeorol. 14 (3), 829–849. http://dx.doi.org/10.1175/jhm-d-12-0107.1.

Döll, P., Fiedler, K., Zhang, J., 2009. Global-scale analysis of river flow alterations due to water withdrawals and reservoirs. Hydrol. Earth Syst. Sci. 13 (12), 2413–2432. http://dx.doi.org/10.5194/hess-13-2413-2009.

ESA, 2017. Land cover CCI product user guide version 2. Tech. Rep., Available at https://maps.elie.ucl.ac.be/CCI/viewer/download/ESACCI-LC-Ph2-PUGv2_2.0.pdf.

FAO, IIASA, ISRIC, ISSCAS, JRC, 2012. Harmonized world soil database (version 1.2). AO, Rome, Italy and IIASA, Laxenburg, Austria.

Frieler, K., Lange, S., Piontek, F., Reyer, C.P.O., Schewe, J., Warszawski, L., Zhao, F., Chini, L., Denvil, S., Emanuel, K., Geiger, T., Halladay, K., Hurtt, G., Mengel, M., Murakami, D., Ostberg, S., Popp, A., Riva, R., Stevanovic, M., Suzuki, T., Volkholz, J., Burke, E., Ciais, P., Ebi, K., Eddy, T.D., Elliott, J., Galbraith, E., Gosling, S.N., Hattermann, F., Hickler, T., Hinkel, J., Hof, C., Huber, V., Jägermeyr, J., Krysanova, V., Marcé, R., Schmied, H.M., Mouratiadou, I., Pierson, D., Tittensor, D.P., Vautard, R., van Vliet, M., Biber, M.F., Betts, R.A., Bodirsky, B.L., Deryng, D., Frolking, S., Jones, C.D., Lotze, H.K., Lotze-Campen, H., Sahajpal, R., Thonicke, K., Tian, H., Yamagata, Y., 2017. Assessing the impacts of 1.5 °C global warming - simulation protocol of the inter-sectoral impact model intercomparison project (ISIMIP2b). Geosci. Model Dev. 10 (12), 4321–4345. http://dx.doi.org/10.5194/gmd-10-4321-2017.

Gan, R., Luo, Y., Zuo, Q., Sun, L., 2015. Effects of projected climate change on the glacier and runoff generation in the Naryn River Basin, Central Asia. J. Hydrol. 523, 240–251. http://dx.doi.org/10.1016/j.jhydrol.2015.01.057.

Gelfan, A., Kalugin, A., Krylenko, I., Nasonova, O., Gusev, Y., Kovalev, E., 2020. Does a successful comprehensive evaluation increase confidence in a hydrological model intended for climate impact assessment? Clim. Change 163 (3), 1165–1185. http://dx.doi.org/10.1007/s10584-020-02930-z.

Gessner, U., Naeimi, V., Klein, I., Kuenzer, C., Klein, D., Dech, S., 2013. The relationship between precipitation anomalies and satellite-derived vegetation activity in central Asia. Glob. Planet. Change 110, 74–87. http://dx.doi.org/10.1016/j.gloplacha.2012.09.007.

Guo, H., He, S., Li, M., Bao, A., Chen, T., Zheng, G., Maeyer, P.D., 2021. Future changes of drought characteristics in coupled model intercomparison project phase 6 shared socioeconomic pathway scenarios over central Asia. Int. J. Climatol. http://dx.doi.org/10.1002/joc.7450.

Hagg, W., Braun, L., Kuhn, M., Nesgaard, T., 2007. Modelling of hydrological response to climate change in glacierized Central Asian catchments. J. Hydrol. 332 (1–2), 40–53. http://dx.doi.org/10.1016/j.jhydrol.2006.06.021.

Hagg, W., Hoelzle, M., Wagner, S., Mayr, E., Klose, Z., 2013. Glacier and runoff changes in the Rukhk catchment, upper Amu-Darya basin until 2050. Glob. Planet. Change 110, 62–73. http://dx.doi.org/10.1016/j.gloplacha.2013.05.005.

Hamidov, A., Helming, K., Balla, D., 2016. Impact of agricultural land use in Central Asia: a review. Agron. Sustain. Dev. 36 (1), http://dx.doi.org/10.1007/s13593-015-0337-7.

Hill, A., Minbaeva, C., Wilson, A., Satylkanov, R., 2017. Hydrologic controls and water vulnerabilities in the naryn river basin, kyrgyzstan: A socio-hydro case study of water stressors in central Asia. Water 9 (5), 325. http://dx.doi.org/10.3390/w9050325.

Hofmeister, F., Arias-Rodriguez, L.F., Premier, V., Marin, C., Notarnicola, C., Disse, M., Chiogna, G., 2022. Intercomparison of Sentinel-2 and modelled snow cover maps in a high-elevation Alpine catchment. J. Hydrol. X 15, 100123. http://dx.doi.org/10.1016/j.hydroa.2022.100123.

Hu, Z., Chen, X., Chen, D., Li, J., Wang, S., Zhou, Q., Yin, G., Guo, M., 2018. “dry gets drier, wet gets wetter”: A case study over the arid regions of central Asia. Int. J. Climatol. 39 (2), 1072–1091. http://dx.doi.org/10.1002/joc.5863.

Hu, Z., Zhang, C., Hu, Q., Tian, H., 2014. Temperature changes in central Asia from 1979 to 2011 based on multiple datasets. J. Clim. 27 (3), 1143–1167. http://dx.doi.org/10.1175/jcli-d-13-00064.1.

Huang, S., Shah, H., Naz, B.S., Shrestha, N., Mishra, V., Daggupati, P., Ghimire, U., Vetter, T., 2020a. Impacts of hydrological model calibration on projected hydrological changes under climate change—a multi-model assessment in three large river basins. Clim. Change 163 (3), 1143–1164. http://dx.doi.org/10.1007/s10584-020-02872-6.

Huang, J., Zhang, G., Zhang, Y., Guan, X., Wei, Y., Guo, R., 2020b. Global desertification vulnerability to climate change and human activities. Land Degrad. Dev. 31 (11), 1380–1391. http://dx.doi.org/10.1002/ldr.3556, arXiv:https://onlinelibrary.wiley.com/doi/pdf/10.1002/ldr.3556, URL https://onlinelibrary.wiley.com/doi/abs/10.1002/ldr.3556.

Huang, A., Zhou, Y., Zhang, Y., Huang, D., Zhao, Y., Wu, H., 2014. Changes of the annual precipitation over central Asia in the twenty-first century projected by multimodels of CMIP5. J. Clim. 27 (17), 6627–6646. http://dx.doi.org/10.1175/jcli-d-14-00070.1.

Huss, M., Hock, R., 2018. Global-scale hydrological response to future glacier mass loss. Nature Clim. Change 8 (2), 135–140. http://dx.doi.org/10.1038/s41558-017-0049-x.

Ibrahim, Y., Balzter, H., Kaduk, J., Tucker, C., 2015. Land degradation assessment using residual trend analysis of GIMMS NDVI3g, soil moisture and rainfall in Sub-Saharan West Africa from 1982 to 2012. Remote Sens. 7 (5), 5471–5494. http://dx.doi.org/10.3390/rs70505471.

Immerzeel, W.W., Pellicciotti, F., Bierkens, M.F.P., 2013. Rising river flows throughout the twenty-first century in two Himalayan glacierized watersheds. Nat. Geosci. 6 (9), 742–745. http://dx.doi.org/10.1038/ngeo1896.

Jiang, L., Bao, A., Jiapaer, G., Liu, R., Yuan, Y., Yu, T., 2022. Monitoring land degradation and assessing its drivers to support sustainable development goal 15.3 in Central Asia. Sci. Total Environ. 807, 150868. http://dx.doi.org/10.1016/j.scitotenv.2021.150868.

Jiang, L., Jiapaer, G., Bao, A., Guo, H., Ndayisaba, F., 2017. Vegetation dynamics and responses to climate change and human activities in Central Asia. Sci. Total Environ. 599–600, 967–980. http://dx.doi.org/10.1016/j.scitotenv.2017.05.012.

Jiang, J., Zhou, T., Chen, X., Zhang, L., 2020. Future changes in precipitation over Central Asia based on CMIP6 projections. Environ. Res. Lett. 15 (5), 054009. http://dx.doi.org/10.1088/1748-9326/ab7d03.

Krysanova, V., Donnelly, C., Gelfan, A., Gerten, D., Arheimer, B., Hattermann, F., Kundzewicz, Z.W., 2018. How the performance of hydrological models relates to credibility of projections under climate change. Hydrol. Sci. J. 63 (5), 696–720. http://dx.doi.org/10.1080/02626667.2018.1446214, URL https://www.tandfonline.com/doi/full/10.1080/02626667.2018.1446214, Number: 5.

Krysanova, V., Hattermann, F.F., Kundzewicz, Z.W., 2020. How evaluation of hydrological models influences results of climate impact assessment—an editorial. 163, (3), pp. 1121–1141. http://dx.doi.org/10.1007/s10584-020-02927-8.

Kundzewicz, Z., Krysanova, V., Benestad, R., Hov, Ø., Piniewski, M., Otto, I., 2018. Uncertainty in climate change impacts on water resources. Environ. Sci. Policy 79, 1–8. http://dx.doi.org/10.1016/j.envsci.2017.10.008.

Kutuzov, S., Shahgedanova, M., 2009. Glacier retreat and climatic variability in the eastern Terskey–Alatoo, inner Tien Shan between the middle of the 19th century and beginning of the 21st century. Glob. Planet. Change 69 (1–2), 59–70. http://dx.doi.org/10.1016/j.gloplacha.2009.07.001.

Lalande, M., Ménégoz, M., Krinner, G., Naegeli, K., Wunderle, S., 2021. Climate change in the high mountain Asia in CMIP6. Earth Syst. Dyn. 12 (4), 1061–1098. http://dx.doi.org/10.5194/esd-12-1061-2021.

Lange, S., 2018. Bias correction of surface downwelling longwave and shortwave radiation for the EWEMBI dataset. Earth Syst. Dyn. 9 (2), 627–645. http://dx.doi.org/10.5194/esd-9-627-2018.

Lange, S., 2019. Trend-preserving bias adjustment and statistical downscaling with ISIMIP3BASD (v1.0). Geosci. Model Dev. 12 (7), 3055–3070. http://dx.doi.org/10.5194/gmd-12-3055-2019.

Lange, S., Menz, C., Gleixner, S., Cucchi, M., Weedon, G.P., Amici, A., Bellouin, N., Müller Schmied, H., Hersbach, H., Buontempo, C., Cagnazzo, C., 2021. WFDE5 over land merged with ERA5 over the ocean (W5E5 v2.0). http://dx.doi.org/10.48364/ISIMIP.342217, URL https://data.isimip.org/10.48364/ISIMIP.342217.

Li, Z., Chen, Y., Li, W., Deng, H., Fang, G., 2015. Potential impacts of climate change on vegetation dynamics in Central Asia. J. Geophys. Res.: Atmos. 120 (24), 12345–12356. http://dx.doi.org/10.1002/2015jd023618.

Luo, M., Liu, T., Meng, F., Duan, Y., Bao, A., Frankl, A., Maeyer, P.D., 2018. Spatiotemporal characteristics of future changes in precipitation and temperature in Central Asia. Int. J. Climatol. 39 (3), 1571–1588. http://dx.doi.org/10.1002/joc.5901.

Lutz, A.F., Immerzeel, W.W., Shrestha, A.B., Bierkens, M.F.P., 2014. Consistent increase in high Asia's runoff due to increasing glacier melt and precipitation. Nature Clim. Change 4 (7), 587–592. http://dx.doi.org/10.1038/nclimate2237.

Ma, X., Zhu, J., Yan, W., Zhao, C., 2021. Projections of desertification trends in Central Asia under global warming scenarios. Sci. Total Environ. 781, 146777. http://dx.doi.org/10.1016/j.scitotenv.2021.146777.

Martens, B., Miralles, D.G., Lievens, H., van der Schalie, R., de Jeu, R.A.M., Fernández-Prieto, D., Beck, H.E., Dorigo, W.A., Verhoest, N.E.C., 2017. GLEAM v3: satellite-based land evaporation and root-zone soil moisture. Geosci. Model Dev. 10 (5), 1903–1925. http://dx.doi.org/10.5194/gmd-10-1903-2017.

Meehl, G.A., Senior, C.A., Eyring, V., Flato, G., Lamarque, J.-F., Stouffer, R.J., Taylor, K.E., Schlund, M., 2020. Context for interpreting equilibrium climate sensitivity and transient climate response from the CMIP6 Earth system models. Sci. Adv. 6 (26), http://dx.doi.org/10.1126/sciadv.aba1981.

Meinshausen, M., Nicholls, Z.R.J., Lewis, J., Gidden, M.J., Vogel, E., Freund, M., Beyerle, U., Gessner, C., Nauels, A., Bauer, N., Canadell, J.G., Daniel, J.S., John, A., Krummel, P.B., Luderer, G., Meinshausen, N., Montzka, S.A., Rayner, P.J., Reimann, S., Smith, S.J., van den Berg, M., Velders, G.J.M., Vollmer, M.K., Wang, R.H.J., 2020. The shared socio-economic pathway (SSP) greenhouse gas concentrations and their extensions to 2500. 13, pp. 3571–3605. http://dx.doi.org/10.5194/gmd-13-3571-2020.

Miralles, D.G., Holmes, T.R.H., Jeu, R.A.M.D., Gash, J.H., Meesters, A.G.C.A., Dolman, A.J., 2011. Global land-surface evaporation estimated from satellite-based observations. Hydrol. Earth Syst. Sci. 15 (2), 453–469. http://dx.doi.org/10.5194/hess-15-453-2011.

Mishra, V., Shah, H., López, M.R.R., Lobanova, A., Krysanova, V., 2020. Does comprehensive evaluation of hydrological models influence projected changes of mean and high flows in the Godavari River basin? Clim. Change 163 (3), 1187–1205. http://dx.doi.org/10.1007/s10584-020-02847-7.

NASA JPL, 2013. NASA shuttle radar topography mission global 3 arc second. http://dx.doi.org/10.5067/MEASURES/SRTM/SRTMGL3.003, URL https://lpdaac.usgs.gov/products/srtmgl3v003/.

Olsson, J., Arheimer, B., Borris, M., Donnelly, C., Foster, K., Nikulin, G., Persson, M., Perttu, A.-M., Uvo, C., Viklander, M., Yang, W., 2016. Hydrological climate change impact assessment at small and large scales: Key messages from recent progress in Sweden. Climate 4 (3), 39. http://dx.doi.org/10.3390/cli4030039.

Ozturk, T., Turp, M.T., Türkeş, M., Kurnaz, M.L., 2017. Projected changes in temperature and precipitation climatology of central Asia CORDEX region 8 by using RegCM4.3.5. Atmos. Res. 183, 296–307. http://dx.doi.org/10.1016/j.atmosres.2016.09.008.

Peña-Ramos, J.A., Bagus, P., Fursova, D., 2021. Water conflicts in central Asia: Some recommendations on the non-conflictual use of water. Sustainability 13 (6), 3479. http://dx.doi.org/10.3390/su13063479.

Peng, Q., Wang, R., Jiang, Y., Li, C., Guo, W., 2021. The change of hydrological variables and its effects on vegetation in Central Asia. Theor. Appl. Climatol. 146 (1–2), 741–753. http://dx.doi.org/10.1007/s00704-021-03730-w.

Poméon, T., Diekkrüger, B., Springer, A., Kusche, J., Eicker, A., 2018. Multi-objective validation of SWAT for sparsely-gauged west African river basins—A remote sensing approach. Water 10 (4), http://dx.doi.org/10.3390/w10040451, URL https://www.mdpi.com/2073-4441/10/4/451.

Rajib, M.A., Merwade, V., Yu, Z., 2016. Multi-objective calibration of a hydrologic model using spatially distributed remotely sensed/in-situ soil moisture. 536, pp. 192–207. http://dx.doi.org/10.1016/j.jhydrol.2016.02.037.

Rasouli, K., Pomeroy, J.W., Whitfield, P.H., 2019a. Are the effects of vegetation and soil changes as important as climate change impacts on hydrological processes? Hydrol. Earth Syst. Sci. 23 (12), 4933–4954. http://dx.doi.org/10.5194/hess-23-4933-2019.

Rasouli, K., Pomeroy, J.W., Whitfield, P.H., 2019b. Hydrological responses of headwater basins to monthly perturbed climate in the North American cordillera. J. Hydrometeorol. 20 (5), 863–882. http://dx.doi.org/10.1175/jhm-d-18-0166.1.

Reyer, C.P., Otto, I.M., Adams, S., Albrecht, T., Baarsch, F., Cartsburg, M., Coumou, D., Eden, A., Ludi, E., Marcus, R., Mengel, M., Mosello, B., Robinson, A., Schleussner, C.-F., Serdeczny, O., Stagl, J., 2015. Climate change impacts in Central Asia and their implications for development. Reg. Environ. Change 17 (6), 1639–1650. http://dx.doi.org/10.1007/s10113-015-0893-z.

Rodell, M., Houser, P.R., Jambor, U., Gottschalck, J., Mitchell, K., Meng, C.-J., Arsenault, K., Cosgrove, B., Radakovich, J., Bosilovich, M., Entin, J.K., Walker, J.P., Lohmann, D., Toll, D., 2004. The global land data assimilation system. Bull. Am. Meteorol. Soc. 85 (3), 381–394. http://dx.doi.org/10.1175/bams-85-3-381.

Saks, T., Pohl, E., Machguth, H., Dehecq, A., Barandun, M., Kenzhebaev, R., Kalashnikova, O., Hoelzle, M., 2022. Glacier runoff variation since 1981 in the upper naryn river catchments, central tien shan. Front. Environ. Sci. 9, http://dx.doi.org/10.3389/fenvs.2021.780466.

Sherwood, S.C., Webb, M.J., Annan, J.D., Armour, K.C., Forster, P.M., Hargreaves, J.C., Hegerl, G., Klein, S.A., Marvel, K.D., Rohling, E.J., Watanabe, M., Andrews, T., Braconnot, P., Bretherton, C.S., Foster, G.L., Hausfather, Z., Heydt, A.S., Knutti, R., Mauritsen, T., Norris, J.R., Proistosescu, C., Rugenstein, M., Schmidt, G.A., Tokarska, K.B., Zelinka, M.D., 2020. An assessment of earth's climate sensitivity using multiple lines of evidence. Rev. Geophys. 58 (4), http://dx.doi.org/10.1029/2019rg000678.

Stephens, C., Marshall, L., Johnson, F., Lin, L., Band, L., Ajami, H., 2020. Is past variability a suitable proxy for future change? A virtual catchment experiment. Water Resour. Res. 56 (2), http://dx.doi.org/10.1029/2019wr026275.

Su, B., Huang, J., Zeng, X., Gao, C., Jiang, T., 2016. Impacts of climate change on streamflow in the upper Yangtze River basin. Clim. Change 141 (3), 533–546. http://dx.doi.org/10.1007/s10584-016-1852-5.

Tebaldi, C., Debeire, K., Eyring, V., Fischer, E., Fyfe, J., Friedlingstein, P., Knutti, R., Lowe, J., O'Neill, B., Sanderson, B., van Vuuren, D., Riahi, K., Meinshausen, M., Nicholls, Z., Tokarska, K.B., Hurtt, G., Kriegler, E., Lamarque, J.-F., Meehl, G., Moss, R., Bauer, S.E., Boucher, O., Brovkin, V., Byun, Y.-H., Dix, M., Gualdi, S., Guo, H., John, J.G., Kharin, S., Kim, Y., Koshiro, T., Ma, L., Olivié, D., Panickal, S., Qiao, F., Rong, X., Rosenbloom, N., Schupfner, M., Séférian, R., Sellar, A., Semmler, T., Shi, X., Song, Z., Steger, C., Stouffer, R., Swart, N., Tachiiri, K., Tang, Q., Tatebe, H., Voldoire, A., Volodin, E., Wyser, K., Xin, X., Yang, S., Yu, Y., Ziehn, T., 2021. Climate model projections from the scenario model intercomparison project (ScenarioMIP) of CMIP6. 12, pp. 253–293. http://dx.doi.org/10.5194/esd-12-253-2021.

Tokarska, K.B., Stolpe, M.B., Sippel, S., Fischer, E.M., Smith, C.J., Lehner, F., Knutti, R., 2020. Past warming trend constrains future warming in CMIP6 models. Sci. Adv. 6 (12), http://dx.doi.org/10.1126/sciadv.aaz9549.

Tuo, Y., Marcolini, G., Disse, M., Chiogna, G., 2018. Calibration of snow parameters in SWAT: comparison of three approaches in the Upper Adige River basin (Italy). Hydrol. Sci. J. 63 (4), 657–678. http://dx.doi.org/10.1080/02626667.2018.1439172.

Unger-Shayesteh, K., Vorogushyn, S., Farinotti, D., Gafurov, A., Duethmann, D., Mandychev, A., Merz, B., 2013. What do we know about past changes in the water cycle of Central Asian headwaters? A review. Glob. Planet. Change 110, 4–25. http://dx.doi.org/10.1016/j.gloplacha.2013.02.004.

Vaze, J., Post, D., Chiew, F., Perraud, J.-M., Viney, N., Teng, J., 2010. Climate non-stationarity – validity of calibrated rainfall–runoff models for use in climate change studies. J. Hydrol. 394 (3–4), 447–457. http://dx.doi.org/10.1016/j.jhydrol.2010.09.018.

Vetter, T., Huang, S., Aich, V., Yang, T., Wang, X., Krysanova, V., Hattermann, F., 2015. Multi-model climate impact assessment and intercomparison for three large-scale river basins on three continents. 6, pp. 17–43. http://dx.doi.org/10.5194/esd-6-17-2015.

Vetter, T., Reinhardt, J., Flörke, M., van Griensven, A., Hattermann, F., Huang, S., Koch, H., Pechlivanidis, I.G., Plötner, S., Seidou, O., Su, B., Vervoort, R.W., Krysanova, V., 2016. Evaluation of sources of uncertainty in projected hydrological changes under climate change in 12 large-scale river basins. Clim. Change 141 (3), 419–433. http://dx.doi.org/10.1007/s10584-016-1794-y.

Wen, S., Su, B., Wang, Y., Zhai, J., Sun, H., Chen, Z., Huang, J., Wang, A., Jiang, T., 2020. Comprehensive evaluation of hydrological models for climate change impact assessment in the Upper Yangtze River Basin, China. Clim. Change 163 (3), 1207–1226. http://dx.doi.org/10.1007/s10584-020-02929-6.

Wilson, A.M., Gladfelter, S., Williams, M.W., Shahi, S., Baral, P., Armstrong, R., Racoviteanu, A., 2017. High Asia: The international dynamics of climate change and water security. J. Asian Stud. 76 (2), 457–480. http://dx.doi.org/10.1017/s0021911817000092.

Wortmann, M., Bolch, T., Menz, C., Tong, J., Krysanova, V., 2018. Comparison and correction of high-mountain precipitation data based on glacio-hydrological modeling in the tarim river headwaters (high Asia). J. Hydrometeorol. 19 (5), 777–801. http://dx.doi.org/10.1175/jhm-d-17-0106.1.

Xenarios, S., Gafurov, A., Schmidt-Vogt, D., Sehring, J., Manandhar, S., Hergarten, C., Shigaeva, J., Foggin, M., 2018. Climate change and adaptation of mountain societies in central Asia: uncertainties, knowledge gaps, and data constraints. Reg. Environ. Change 19 (5), 1339–1352. http://dx.doi.org/10.1007/s10113-018-1384-9.

Xing, X., Qian, J., Chen, X., Chen, C., Sun, J., Wei, S., Yimamaidi, D., Zhanar, Z., 2022. Analysis of effects of recent changes in hydrothermal conditions on vegetation in Central Asia. Land 11 (3), 327. http://dx.doi.org/10.3390/land11030327.

jie Xu, H., ping Wang, X., xiao Zhang, X., 2016. Decreased vegetation growth in response to summer drought in Central Asia from 2000 to 2012. Int. J. Appl. Earth Obs. Geoinf. 52, 390–402. http://dx.doi.org/10.1016/j.jag.2016.07.010.

Zhang, G., Biradar, C.M., Xiao, X., Dong, J., Zhou, Y., Qin, Y., Zhang, Y., Liu, F., Ding, M., Thomas, R.J., 2018. Exacerbated grassland degradation and desertification in Central Asia during 2000–2014. Ecol. Appl. 28 (2), 442–456. http://dx.doi.org/10.1002/eap.1660.

Zhou, Y., Zhang, L., Fensholt, R., Wang, K., Vitkovskaya, I., Tian, F., 2015. Climate contributions to vegetation variations in central Asian drylands: Pre- and post-USSR collapse. Remote Sens. 7 (3), 2449–2470. http://dx.doi.org/10.3390/rs70302449.